Forced Folding in the Kora Volcanic Complex, New Zealand: A case study with relevance to the production of hydrocarbons and geothermal energy

Priyadarshi Chinmoy Kumar[1, a], Tiago Alves[2, b] and Kalachand Sain[1, c]

[1]Wadia Institute of Himalayan Geology, Dehradun, Utrakhand, India
[2]3D Seismic Lab, Cardiff University, Cardiff, UK
[a]kumarchinmoy@gmail.com; [b]alvest@cardiff.ac.uk; [c]kalachandsain7@gmail.com
Corresponding Author: kumarchinmoy@gmail.com; chinmoy@wihg.res.in

Abstract

Magma intrusion into relatively shallow strata often results in intense structural deformation in host strata. Forced folds are typical formed above the intrusions in order to accommodate the addition of new volumes of magma into the sedimentary pile. This work uses a high-resolution 3D seismic volume from the offshore Taranaki Basin, New Zealand to investigate large forced folds formed in Upper Cretaceous-Paleocene sequences due to the intrusion of a series of magmatic dikes and sills. These magmatic intrusions are related to the plumbing system of the Kora Volcano. We apply a novel filtering technique to enhance the contrast between the dip-azimuth of seismic reflectors and that of any overprinting noise, preserving the lateral continuity of seismic events. Forced folds were generated due to the intrusion of flat-laying saucer-shaped sills into shallow strata. These folds (Fold A and Fold B) have a domal geometry and a structural relief of 250-350 m, for a total area of 45 km^2 and 35 km^2, respectively. Out of the 18 interpreted sills, two sills (S1 and S4) contributed the most to the generation of the forced folds in the study area. The sill-fold relationships observed in this work suggest that sills with greater length-to-intrusion ratios deform the strata more effectively. Importantly, forced folding led to the development of four-way closures understood to form prolific traps for hydrocarbon and geothermal energy resources.

Keywords: New Zealand; Taranaki Basin; Forced folds, Magmatic sills, Geoenergy exploration, Kora volcano

1. Introduction

Forced folds in sedimentary basins, defined as structures developed due to the intrusion of magma into host strata, are commonly associated with interconnected networks of magmatic sills (Smallwood and Maresh, 2002; Hansen and Cartwright, 2006b; Cukur et al., 2010; Magee et al., 2013; 2014; Alves et al., 2015; Omosanya et al., 2017). Earlier work on forced folding was mainly based on detailed field observations to address the two-dimensional geometry of such structures (du Toit, 1920; Loewinson-Lessing, 1936; Tweto, 1951; Hotz, 1952; Pollard and Johnson, 1973; Stearns, 1978). However, these early publications were clearly limited in terms of understanding the 3D geometry of forced folds and their relation to adjacent magmatic sills. With the advent of 3D seismic data authors such as Hansen et al. (2004), Trude et al. (2003), Cartwright and Huuse (2005) and Hansen and Cartwright (2006b) have studied magmatic intrusions in great detail. However, due to the common reduction in signal strength (and limited processing of data) at the depth of occurrence of igneous intrusions and forced folds, the seismic imaging of such geological features should be enhanced to properly quantify and characterise them(e.g. Eide et al., 2017; Kumar et al., 2019a,b).

At a local scale, forced folds generate accommodation space for intruded magma sourced from the deeper parts of the crust and upper mantle (Pollard and Johnson, 1973;

Hansen and Cartwright, 2006b; Jackson et al., 2013; Montanari et al., 2017). The subsurface movement of magma also affects surrounding host-rock fluids and mineralisation, increasing interstitial water temperature to create supercritical conditions for fluid circulation (Scott et al., 2015). In parallel, the presence of fault and fracture systems within forced folds generates new pathways for the migration of superheated and supercritical fluids (Weis, 2015; Scott et al., 2015), at the same time controlling the relative strain experienced by overburden strata during their uplift (Pollard and Johnson, 1973; Hansen and Cartwright, 2006b; Jackson et al., 2013).

Recent work suggest that super-heated and critical fluids comprise economic geothermal resources well-suited for energy production (Friðleifsson et al., 2014; Liotta et al., 2015; Sani et al., 2016; Montanari et al., 2017; Bischoff, 2019). The first attempt at producing geothermal energy from supercritical fluids was made during the Iceland Drilling Project (2009-2012) (Friðleifsson et al., 2014). Together with geothermal exploration in Iceland, the Larderello-Travale and Elba Island geothermal fields in Tuscany, Italy, have gained much attention as producers of geothermal energy (Liotta et al., 2015; Sani et al., 2016). Furthermore, notable examples of hydrocarbon prospects associated with forced folds above magmatic sills include: (1) the Wichian Basin in Thailand (Schutter, 2003); (2) the Northern Sub-basin, Offshore Senegal (Hansen et al., 2008); (3) the Møre Basin, offshore Norway, where a folded carbonate reservoir lies above the Tulipan Sill (Polteau, 2008); (4) the Neuquén Basin in Argentina (Rodriguez Monreal et al., 2009); (5) the Exmouth Sub-basin offshore NW Australia (Magee et al., 2013a); (6) the Bight Basin offshore Southern Australia (Jackson et al, 2013); (7) the Irish Rockall Basin, offshore NE Ireland (Magee et al., 2014); and (8) the Faroe-Shetland Basin, NE Atlantic (Schofield et al., 2017). A detailed mapping of forced folds and associated magma intrusions is critical to de-risk both geothermal and hydrocarbon prospects with proven economic value.

The magmatic province of Taranaki Basin, offshore New Zealand, hosts a chain of buried submarine strato-volcanoes that were active during the Miocene period (Herzer, 1995; King and Thrasher, 1996; Bischoff et al., 2017; Morley, 2018; Kumar et al., 2019a, b). In particular, the Kora Volcanic Complex (Figs. 1a-c) has been an area of interest to multiple researchers (Herzer, 1995; King and Thrasher, 1996; Bischoff et al., 2017; Morley, 2018; Infant-Peaze and Marfurt, 2018; Kumar et al., 2019a; b). Petrogenetic models proposed by Bergman et al. (1992) demonstrate that magma feeding the Kora Volcanic Complex originated ~100 km deep, where the dehydration of the subducting Pacific plate beneath the Australian plate induces adiabatic melting of the asthenosphere. The magma rose into the crust through a network of magmatic sills that intruded both shallow and deep levels of the crust. Such intrusions structurally deformed Upper Cretaceous-Paleocene strata in the Taranaki Basin to generate forced folds above them. As a result, this paper aims to investigate: (i) the structures and geometries of forced folds developed above selected magmatic sills in the Kora prospect; (ii) the dimensions of forced folds formed in association with the intrusion of sills, and (iii) how accurately can these structures be imaged and interpreted using enhanced seismic data.

Based on the results of this work, we propose a conceptual model explaining the growth and development of forced folds, and resulting uplift of the overburden enclosing such magmatic sills. This work will improve our understanding about the mechanisms that form forced folds above magma intrusions, as many of these structures can form viable traps for geothermal heat and hydrocarbons.

2. Geological setting

The Taranaki Basin is the main hydrocarbon-rich basin in New Zealand (King and Thrasher, 1996) and lies to the west of the North Island (Figs. 1a and b). The Taranaki Basin lies about ~400 km west of the Hikurangi Trough, where the Pacific plate is subducted beneath the Australian plate (King and Thrasher 1996Giba et al. 2010). The basin is ~60 km wide and extends ~350 km in a NNE direction from the southern Taranaki Peninsula to the offshore area to the west of Auckland (Giba et al., 2010).

The tectonic development of the basin dates from the Late Cretaceous, when the breakup of Gondwanaland and subsequent formation of the Tasman Sea originated fault-bounded graben and half-graben structures (King and Thrasher, 1996; Higgs et al., 2012). These structures were filled with syn-rift strata consisting of interbedded coal and sandstone, part of the Pakawau Group (Fig. 2; Palmer and Andrews 1993; King and Thrasher 1996). Overlying Paleocene and Eocene deposits are late-rift and post-rift transgressive sequences (King and Thrasher 1996; Higgs et al. 2012). These deposits contain terrestrial to marginal marine sequences in the Kapuni Group, i.e. the Farewell, Kaimiro, Mangahewa and McKee formations (Higgs et al., 2012; Kumar et al., 2019a). Tectonic quiescence and a relative reduction in clastic sediment input to the basin during the Oligocene led to widespread deposition of limestones and calcareous mudstones in the Ngatoro Group (Otaraoa and Tikorangi Formations) (King et al., 1999; King 2000). This transgressive phase reached its climax in the Early Miocene (Ngatoro and Wai-iti Groups), anticipating the start of a regressive phase that lasted from the Middle Miocene (Wai-iti Group) to the Pliocene-Quaternary (Fig. X).

2.1 Structure of the Kora Volcanic Complex

The Kora Volcanic Complex lies within the NNE-trending Mohakatino Volcanic Belt (MVB), a belt of igneous edifices and sills that lies close to the Northern Taranaki Graben (NTG), offshore Taranaki Basin (Fig. 1c). The Mohakatino Volcanic Belt contains a chain of buried submarine volcanoes that are part of an intraarc magmatic system developed due to dehydration of the westward subducting Pacific plate beneath the Australian plate (King and Thrasher, 1996; Seebeck et al., 2014; Bischoff et al., 2017; Kumar et al., 2019b). The study area is well-known for successfully producing over 1168 barrels of oil per day (bopd) for about 10 days within a thick sequence of Miocene volcaniclastic rocks when drilled for a production test by the Kora-1 well (ARCO, 1988). The magma into the well-known Kora volcano, on which the Kora-1 well was drilled, was fed from asthenospheric mantle via a plumbing system consisting of dyke swarms and sill networks (Stagpoole and Funnel, 2001; Bischoff et al., 2017; Morley, 2018; Kumar et al., 2019b). As a result, the intrusion of magma in this area resulted in uplift and deformation of Upper Cretaceous to Paleocene strata around the Kora Volcanic Complex (Stagpoole and Funnel, 2001; Morley, 2018). Volcanic eruptions in the study area are estimated to have begun c. 18 Ma, continuing until c. 8 Ma (Bergman et al., 1992; King and Thrasher, 1996). Later, volcanic activity ceased and the Kora volcano was onlapped by thick prograding marine sediments of the Giant Foresets Formation (Bergman et al., 1992; King and Thrasher, 1996; Stagpoole and Funnel, 2001; Bischoff et al., 2017; Bischoff, 2019; Kumar et al., 2019b).

2.2 Subsurface lithology around the Kora Volcanic Complex

The subsurface lithostratigraphy of the study area comprises sedimentary units deposited from the Late Cretaceous to the Holocene (Fig. 4). The Kora-1 well drilled through the Giant Foresets Formation to reach the flanks of the so-called Volcanic Formation (Fig. 4b). The well crossed the Eocene-Oligocene Tangora sandstone to reach on the top of the Eocene Kaiata interval, at a measured depth of 3421 m (ARCO Petroleum Kora-1 Well Completion Report, 1988).

The Kaiata Formation (KF) is a shale unit interbedded with siltstone, sandstone and limestone. Above this unit lie turbiditic sandstones interbedded with limestones and occasional claystones, part of the Tangaroa Formation (Fig. 4b). Miocene strata comprise the Volcanic Formation, well-known for the faulted (and conical) Kora volcano. The well completion report for well Kora-1 suggests that this volcanic interval has fair to good porosity and permeability, justifying the oil shows found at depths between 1785 m and 1810 m (ARCO Petroleum Kora-1 Well Completion Report, 1988). Magmatic activity was particularly intense in the study area during the Miocene, and is associated with the eruption of the Kora volcano (Fig. X).

3. Data and Methods

The data used in this study include a depth migrated 3D seismic volume with 782 inlines (Lines no. 888 to 1670) and 1584 xlines (Lines no. 978 to 2562) (Fig. 1c). The seismic volume was acquired by the M/V Orient Explorer in March 2005 and covers an area of ~ 750 km^2 (OMV New Zealand Report, 2005). Data acquisition included the definition of a bin size of 25 m by 12.5 m, the selection of a 66-fold data coverage, and a 6.0 s record length. The primary goal of the 3D seismic survey was to provide improved images of the Eocene Tangaroa sandstone unit, at the same time resolving the spurious ray-path geometries associated with the Kora volcano (OMV, 2005).

The seismic data were processed using routine processing workflows that included trace edits, noise, multiple attenuation, velocity analysis and NMO correction, followed by post stack Kirchhoff time migration. Later, the outputs from time-domain processing flows were used to prepare a depth-migrated seismic cube. The depth migration included updating the seismic velocity models using iterative methods, a full Kirchoff depth migration, residual move-out (RMO) corrections, automatic time varying RMOs followed by a final mute, exponential signal gains and a post stack filtering. The data length of the depth migrated seismic cube is 8 km.

Earlier research (e.g., Bischoff et al., 2017; Infante-Paez and Marfurt, 2017; Morley, 2018; Kumar et al., 2019a; b; Bischoff and Nicol, 2019; Bischoff et al., 2020) investigated the Kora prospect using time-migrated seismic cubes, opacity rendering and geobody interpretation techniques. The limit of vertical resolution as suggested by these studies is 55 m, i.e., only magmatic sills thicker than this value can be resolved by the seismic volumes previously used (Morley, 2018; Kumar et al., 2019a; b). Here, we use a newly prepared depth-migrated seismic cube procured for academic research from New Zealand Petroleum and Minerals (NZP&M). This depth-migrated volume was deemed a better option for interpretation as one can directly and accurately compute several morphometric parameters (e.g., thickness, length, area, etc.) of volcanic features rather having to use velocity data to convert time to depth. These new data are displayed using the SEG's American polarity convention whereby an increase in acoustic impedance is represented by a peak (a positive- amplitude black reflection) on seismic profiles.

In order to improve the resolution of volcanic features at depth, the depth-migrated seismic cube was structurally conditioned using a structure-oriented filter (SOF), defined as

the dip-steered median filter (DSMF), which was earlier applied successfully in other offshore prospects by Kumar et al. (2019a;b;c). The DSFM applies median statistical parameters over seismic amplitudes following the observed seismic dips. The filtering was performed using a mild 3x3 median filtering step-out. The key objective behind this filtering technique is to differentiate between the dip-azimuth of seismic reflectors and overprinting noise (Chopra and Marfurt, 2007), therefore removing random noise from the data while preserving the amplitudes and enhancing the lateral continuity of seismic events. In order to determine the structural architecture of igneous intrusions, extrusive bodies, induced forced folds and other discontinuous structures, different seismic attributes such as dip angle, azimuth and energy gradient were computed and colour blended to observe the structural complexities associated with the picked Late Cretaceous-Paleocene seismic Horizon A. In addition, geobody extraction was followed by opacity rendering techniques (Alves et al., 2015; Bischoff et al., 2017) to visualise and interpret structural architecture of magmatic sills.

Approximately 18 sills showing distinct geometries were identified below the forced folds considered in this work. Their morphometric properties such as length, width, aspect ratio, thickness and orientations, were interpreted in map view and in selected seismic profiles crossing the centre of the mapped sills (Fig. 3). Fold diameter (FD), fold amplitude (FA) and limb dips were estimated from these selected seismic profiles (Fig. 3). These parameters were used to compile different graphs from which the shape, structural relief and overall geometry of the forced folds were ascertained. In parallel, different morphometric plots were prepared to understand sill-fold relationships. After performing a detailed analysis, a conceptual model was proposed to demonstrate the growth and development of forced folds.

4. Results

Magma ascent took place from an upper crustal magma chamber via a plumbing system consisting of dyke swarms and interconnected sill networks, thereby cross-cutting and intruding the deposited sedimentary sequences (Morley, 2018; Kumar et al., 2019a; b). Their intrusion deformed and uplifted strata both at deeper and shallower levels. This research focuses on Upper Cretaceous-Paleocene strata lying below the Kaiata interval, from 4.5 km and 7.0 km depth, in which magmatic sills uplifted the surrounding strata to generate multiple forced folds (Fig. 4b).

4.1 Interpretation of magmatic sills

Magmatic sills within the Upper Cretaceous-Paleocene interval show distinct geometries, of which the most common are saucer-shaped bodies and inclined sheets occurring in isolation or interconnected with junctions, as shown in Figs. 5 and 6. The interpreted magmatic sills (n=18) in this interval show thicknesses ranging between 57 m and 150 m, and aspect ratios (AR) ranging from 0.9 to 2.4 and areas <5 km^2. The sills were intruded at depths 250-460 m below Horizon A, which is structured with two major domal features named Fold A and Fold B. In addition, the detailed morphometric parameters for the interpreted sills are shown in Table 1.

4.1.1 Magmatic sills intruded below Fold A

The area around Fold A region is intruded by sills S1-2, S11-12 and S15-18. Sills S1 and S2 are saucer-shaped, concordant with the bedding, and reveal a concave morphology with transgressive discordant limbs (Figs. 5c and g). The limbs of sill S2 extend outwards

from the inner surface in multiple steps. Both sills S1 and S2 trend NE-SW and occur at depths of 230-510 m below Fold A. Sill S11 shows a typical saucer-shaped geometry with one of the limbs transgressing upwards to the host strata (Figs. 5e and i). The other limb laterally spreads out with steps. Sill S12 occurs in isolation.

Sills S15 and S16 are sheet-like intrusions trending N-S and inclined at angles of 59^{o} and 48^{o}, respectively. Sills S17 and S18 remain isolated towards the SE part of the study area. They are structured with flat base and their limbs transgress upwards with a stepped geometry (Figs. 5f, 5j, 6f and 6j).

4.1.2 Magmatic sills intruded below Fold B

The area around Fold B region is intruded by sills S3-10 and S13-14. Sill 3 shows a similar geometry to sills S1 and S2 (Figs. 5d, 5h, 6c and 6g). Sill S4 is made up of equally-spaced magma lobes arranged in en-echelon steps (Figs. 6d and 6h). Its geometry can be appreciated in more detail in Fig. 7, where these en-echelon steps are connected by bridges (Schofield et al., 2012). Sill S5 is a sheet-like intrusion where the limb is inclined at an angle of 56^{o} and the sill strikes to N (Figs. 5d and 5h). The limb at the base rests upon sill S6, thereby demonstrating a developed “B-type” junction (Hansen and Cartwright, 2006a). Sill S7 is saucer-shaped and is linked to sill S3 at its base, revealing a “B-type” junction. Sills S8 and S9 are inclined sheet-like intrusions, while sill S10 shows an inverted saucer shape and strikes to the NEE (Figs. 5d and h). Sills S13 and S14 display a flat base with limbs connected in several steps. The limb of sill S13 rests over the limb of sill S14, thereby revealing a “B-type” junction between these two sills (Figs 5e and 5i). Both sills trend NE-SW. The limbs of Sill S14 are connected to the flat base through steps and bridges (Figs. 6e and j).

Opacity rendering demonstrates that sills S4 and S14 have broken-bridge structures (Nicholson and Pollard, 1985; Bussell, 1989; Hutton, 2009; Schofield, 2012). In S4, one observes that the magma flowed as a series of en-echelon bodies associated with steps but continuous seismic reflections (Figs. 7a, 7c and 7g). Such broken-bridge structures are observed on either side of sill S4, indicating the presence of continuous host-strata failure during the injection of magma (Figs. 7a, 7f and 7j). Sill S14 also displays broken bridges as shown in Figs. 7b and 7k-r. In S14, magma moved in steps (Figs. 7b, 7k and 7o). The inflation of magma bent the bridge leading to the rupture of these broken-bridge structures, deforming sill S14 at the same time (Figs. 7b and 7l-q).

4.2 Forced folding as a consequence of sill intrusion

Seismic Horizon A is folded immediately above the interpreted magmatic sills. Two major domal features, named as Fold A and Fold B are observed within this horizon, which is overlain by the Eocene and Oligocene-Miocene strata (Figs. 4 and 8). Fold A lies in the central part of the study area, while Fold B occurs at a distance of 5 km from Fold A, towards the NW (Figs. 4 and 8).

Fold A has a semi-circular geometry in map view, with limbs dipping between 5^{o} and 29^{o} (Fig. 8a). The crest of the fold is deformed and elongated to the NE and NW, while its SE and SW limbs are faulted. The fold lies directly above sills S1 and S2; S1 lies ~240 m below the fold crest in the central part and S2 lies ~490 m below the fold (Fig. 5b). Fold A displays a maximum structural relief (fold amplitude) of ~335 m, a diameter of ~3 km, and covers an area of ~45 km^{2} (Fig. 8a and Table 2).

Fold B is semi-circular in map view away from its crest, and its limbs dip between 10^{o} and 28^{o} (Fig. 8a). The fold is underlain by sills S3, S4 and steep sheet intrusions (Fig. 6b). It reveals a maximum structural relief of ~290 m, a diameter of ~1.98 km, and covers an area of ~35 km^2 (Fig. 8a and Table 2).

4.4. Geometry and dimensions of sill-related forced folds

The graphs in Fig. 9a-d show that the crest of Fold A is semi-circular but undulated, likely a result of the multiple intrusions of magma observed in the study area, rather than a single one. The fold resembles an elongated arch, initiating with a gentle dip on its limbs (Fig. 9b). In the central part of the fold i.e., towards the crest, the limb of the fold is steep, becoming broader (Fig. 9c). The limb of Fold A has a maximum dip of 16^{o}. Fold amplitude increases proportionally to the thickness of sill S1 suggesting that the intrusion of the sill forcefully uplifted the surrounding strata (Fig. 9d). The maximum thickness of Sill 1 is observed in its central part (~150m), where the amplitude of Fold A is the greatest (~335m).

The relationship between the thickness of the mapped sills (S1-18) and the structural relief of Fold A was further analysed by compiling plots of fold amplitude vs. sill thickness (Fig. 10). Out of the 18 mapped sills, one observes that the thickness of sill S1 and the relief of Fold A demonstrate a direct relationship, with a coefficient of determination (R^2) of ~88% (Fig. 10). Furthermore, Fold B reveals an overall semicircular geometry (Figs. 11a-d). The cross-section of the fold resembles an inclined ladder with steps. The limbs of Fold B show a maximum dip of 19^{o} (Fig. 11d).

From Figs. 7a and 7c-j it is clear that sill S4 is made up of equally spaced magma lobes containing broken bridge structures. Sill S4 has a maximum thickness of ~87m, and generated a forced fold (Fold B) with a maximum structural relief of ~290 m (Figs. 11a-d). In comparison to Fold B, the limbs of Fold A are more intensely faulted as observed in the colour-blended attribute map in Fig. 12a. In the western part of the Fold A, faults are concentric to radial with en echelon patterns (Figs. 12a, 12b and 12e). In the eastern part of Fold A, the limb is intensely faulted and associated with closely-spaced extensional faults, as observed in the attribute blended map and seismic profiles in Figs. 12a and 12(c-g). In this region, the faults show a polygonal geometry. The presence of these structures suggest that strain experienced during the folding process was accommodated by a set of extensional faults (e.g. Bischoff et al., 2017) developed at the level of stratigraphic Horizon A.

5. Discussion

5.1: Multiple sill intrusions and its effect on the geometry and architecture of forced folds

Several pioneering works pertaining to forced folds due to emplacement of magmatic bodies have been reported from field observations, lab experiments and interpretation of seismic reflection data (e.g., du Toit, 1920; Hotz, 1952; Stearns, 1978; Tweto, 1951; Pollard and Johnson, 1973; Cosgrove, 2000; Cosgrove and Ameen, 2000; Trude et al., 2003; Galland et al., 2004; Hansen et al., 2004; Cartwright and Hansen, 2006; Cukur et al., 2010; Alves et al., 2015; Magee et al., 2013; Omosanya et al., 2016). Around the Kora Volcanic Complex, the presence of such folded structures has been previously documented by authors such as Bischoff et al. (2017), Infante-Paez and Marfurt (2017), Morley (2018), Kumar et al. (2019 a;b). Most of these folds were interpreted as affecting Eocene-Miocene strata. The present work identifies the presence of folds at deeper stratigraphic levels, i.e. affecting the Upper

Cretaceous-Paleocene strata, with Upper Cretaceous units being intruded by a network of magmatic sills and dikes. Bischoff and Nicole (2019) and Bischoff et al. (2020) reported that most of the magmatic intrusions occur in Cretaceous grabens within the Taranaki Basin.

Previous studies have suggested that the uplift of the strata is governed by the ratio between the sill diameter (or length) and the depth of intrusion, named the L/D ratio by Pollard and Johnson (1973), Fialko et al. (200) and Hansen and Cartwright (2006). This ratio represents the empirical fact that sills having larger L/D ratios will greatly deform the overburden when compared to those sills with smaller L/D ratios. Furthermore, earlier studies reported the influence of single magmatic sills in deforming the overburden (Fialko, 2001; Hansen and Cartwright, 2006b; Galland et al., 2009; Jackson et al., 2013; Agirrezabala, 2015). The present research shows that the Forced Folds A and B are underlain by a network of magmatic sills (S1-S18). In such a setting, it is important to investigate the contribution of each of these sills to the generation of the two forced folds.

We observe that sills S1-2, S11-12 and S15-18 are emplaced below Fold A. The L/D ratio of these sills varies between 6.4 and 0.9 (Fig. 13a). Sill S1 is intruded at a depth of ~240 m below Fold A and shows an L/D ratio of ~6.4 (Fig. 13a). The L/D ratio decreases for sills S11, S12, S15, S17 and S16. Sills S12 and S17 record the smallest L/D ratio at ~0.9 (Fig. 13a). Thus, the L/D criteria (L/D>1) of Fialko (2001) fails for S11-S12 and S15-S18, as the estimated length to intrusion depth ratio for these sills falls below 1. This suggests that these sills continued to propagate horizontally into the surrounding strata and may not have turned towards the free surface lying above them. Hence, their contribution to deform the Fold A area is significantly smaller. However, as the L/D criteria is more significant for S1 than S2, the contribution of S2 to deforming Fold A is relatively small. The impact of S1 on Fold A is observed to be the largest, is relatively small for S2 and becomes ever-so small for S11-12 and S15-18 (Fig. 4). In Fold A, bending is chiefly observed in its crestal zone with the fold widening along its limbs (Fig. 5). The presence of extensional faults along the limbs of Fold A further accommodated strain during the widening process (Fig. 5).

The area around Fold B is intruded by sills S3-14. The L/D ratio of these intruded sills varies between 2.5 and 0.5 (Fig. 13b). Sill S4 records the largest L/D ratio of 2.5, while sill S7 shows the smallest at 0.5 (Fig. 13b). This suggests that, out of the observed sill network sill S4 (presently at a depth of ~310 m) contributed the most to generating Fold B (Fig. 6). This contribution is relatively small for S3 and S9, where the L/D is ~2.0. It gradually decreases for S5, S8 and S13 (~1.2-1.4) and further decreases (~0.5) for S6, S7, S10 and S14. Hansen and Cartwright (2006b) emphasised that the geometry of magmatic sills plays a significant role in controlling the structural relief of forced folds above them. In this regard, the saucer shape of the sills fully contributes to the forced folding of overlying strata. Though sills S1 and S4 are associated with Folds A and B, Fold A has greatest structural relief when compared to Fold B. This is because of the fully developed saucer-shaped geometry of sill S1 as compared to sill S4, the latter of which generated Fold B.

5.2 Growth of forced folds above saucer-shaped sills

Theoretical models and observations in Fialko (2001) demonstrated that an increase in the L/D ratio of sills initially deforms the intrusion roof. Later, stress perturbations prevailing on the overlying free surface, rotate the sill trajectory towards the free surface causing the vertical displacement of strata. The limiting condition that makes an intruded sill to turn towards the overlying strata is a length-to-depth of intrusion (L/D) ratio >1 (Fialko, 2001). Upon attaining this condition, the stress concentration towards the tip of the sill is amplified and the growth of

the sill becomes asymmetric, propagating towards the free surface. The sill continues to climb up and, after a length three times the intrusion depth is reached, interactions with the overlying bounding surface start to occur. Subsequently, the surface bends and deforms to accommodate the intruded magmatic fluids (e.g. Malthe-Sorensen et al., 2004). Experimental modelling of shallow magma emplacement by Galland et al. (2004) demonstrate that when the L/D ratio becomes ~1.5 an inclined sheet within the sill develops and deflects the tip of the sill upwards; this phenomenon initiates the deformation of the overburden strata. In parallel, observations by Hansen and Cartwright (2006b) from NE Rockall confirmed that, upon attaining a length of two to four times the intrusion depth, sills transgress by deflecting their tips upwards; the increased interaction with the free surface causes an upward displacement of the host rock in which the sills intrude. Sigmundsson et al. (2018) documented that surface deformation caused by magma emplacement depends on the movement of magma per se. Further, the models of deformation for magmatic sills presented by Sigmundsson et al. (2018) are also in agreement with Fialko (2001). Thus length-to-depth of intrusion (L/D) ratio plays a significant role in estimating the magnitude of overburden deformation caused by sill intrusions.

In the study area we observe that out of the 18 mapped sills, S1 is the sill that contributes the most to generating Fold A (Fig. 13a). Sill S1 is a fully developed saucer-shaped sill, but the interpretation of seismic profiles in Figs. 14a and 14d suggest that, initially, S1 had a flat geometry. As the sill started to spread laterally, there was an increase in its length at about six times the depth of intrusion, resulting in its asymmetric structure – a combination of concave base and rising-upward limbs (Figs. 14b and 14e). Upon reaching a maximum limit at the edges of the fold, shear stress made the sill tip transgress upwards to affect the free surface below the fold (Figs. 14b and 14e). The consequence of such a sequence of events is the development of Fold A (Figs. 14c and f).

The L/D ratio for sill S2 approaches 4.8, suggesting that this sill is also a developed saucer-shaped sill. However, S2 occurs at a depth ~510 m, i.e. deeper than the present depth of sill S1, suggesting that the impact of S2 is relatively small. This reveals that the intrusion of sills at shallow levels in the crust has a greater impact in deforming the host strata.

Other sills such as S11, S12, S15, S16, S17 and S18, intruded in deeper strata, resemble a flat geometry in which their saucer-shape is not well developed and the sill tips remain static. Moreover, their contribution in deforming Fold A gradually decreases to become minor for S11-S12 and S15-S17, the deepest sills in the study area.

Out of the intruded sills in the NW part of the Kora Volcanic Complex, it is observed that sill S4 has a length ~2.5 times the intrusion depth and contains en echelon magmatic lobes further resembling broken-bridge structures (Figs. 15a-l). Gradually, as the magma inflated, the bridges between the lobes were bent and deformed (Figs. 7a, 7d and 7h). With the increase in the flexure of the bridge, and continuous inflation of magma, the bridge experienced failure and developed the broken bridges (Figs. 7a, 7e and 7i). The movement of these magmatic lobes into the surrounding host and subsequent interactions, may not only create the necessary conditions to form supercritical fluids but also has uplifted the host generating Fold B (Figs. 15a-l). Though Fold B is also related to the intrusion of sills S3-S14, the contribution of S4 is significant to its formation.

5.3 A conceptual model explaining the generation of forced folds

The interpretations carried out in this research are valid additions to the earlier proposed models of Fialko (2001), Malthe-Sorensen et al. (2004), Hansen and Cartwright (2006b) and Galland et al. (2009). Our results show that for a saucer-shape structure to be fully developed

as a sill, such that it can continuously climb up to fold the host strata, the length of the intrusion not only need to exceed the depth of intrusion (L/D ratio) by a factor of two to four (Fialko, 2001; Malthe-Sorensen et al., 2004; Hansen and Cartwright, 2006b), but may also be as high as six (6). Earlier models considered the role of magmatic sills in isolation to deforming the host strata and generate forced folds. Our results demonstrate that the cause of such deformation should not only be correlated to a single magmatic sill – networks of sills can also deform the overburden, with each of the discrete sills contributing to deforming the host strata to generate broader forced folds. We further confirm the fact that sills intruded at shallow levels in the study area have greater impact in deforming the host strata, compared to those intruded at deeper levels.

Based on the data in this work, a three stage model explaining the growth and development of forced folds is suggested in Fig. 15a-c. In the first stage, multiple layer-parallel intrusions (or sills with a flat base) tries to intrude the overlying strata at different depths (Fig. 16a). In a second stage, as each of these sills grows and spreads by increasing their diameter, shear stress controls their layer-parallel geometry (Fig. 16b). As their sizes increases to 2-6 times the depth of intrusion, the limbs start transgressing upwards to form a 'typical' saucer shape, at the same time deforming the free surface below its overburden. In a third stage the limbs keep transgressing and, upon the interaction with the surrounding free surface, vertical displacement of the overlying bed ensues (Fig. 16c). At this stage, each sill contributes individually to deforming the overburden. Sills with larger L/D ratio are more significant deforming the overburden strata; those with very low L/D ratios are less important. Towards the tip, as the sill thins out, the fold produces gently dipping limbs outlining the overall structural geometry of the forced fold. In parallel, the presence of faults along the limbs of the forced fold accommodates the strain experienced during the folding process.

5.3 Structural conditioning: a method to improve the imaging of hydrocarbon and geothermal traps

The interpretation of intruded sill networks and related forced folds becomes harder when seismic data show large amounts of coherent and random noise. Seismic data with noisy returns reveal a marked decrease in their signal-to-noise ratio (s/n), reducing the accuracy of several corrections during the processing stage and, ultimately, degrading the quality of the processed data (Liu et al., 2006; Kumar et al., 2019a; b; c). Magee et al (2015) and Eide et al. (2017) demonstrated that presence of random noise in seismic data results into poor recognition of sill networks and associated structures. Hence, structural conditioning of the data is a possible way to circumvent such problems.

In this work, the interpreted depth-migrated seismic volume was conditioned using a structure oriented filter (SOF) applied on a pre-processed steering cube that stores dip/azimuth information at every sample location in the data. Structural conditioning of the data resulted in a conditioned seismic cube named the Dip Steered Median Filtered (DSMF) volume. Within this DSMF volume, amplitude content throughout the geologic targets becomes laterally continuous, random noise is supressed and the s/n ratio is improved. As a result, the visibility of magmatic sills and associated structures is improved, as so is the interpretation process (Fig. 17a-d).

Forced folds can contribute to forming hydrocarbon traps when associated with four-way-dip closures. The strata packages lying above the horizons interpreted in this work are known reservoir intervals around the Kora Volcanic Complex; the Eocene-Oligocene

Tangaroa sandstones (Fig. 4b). Moreover, Bischoff et al. (2017) also documented that the movement of magma into the shallow sedimentary strata and eruptions of the well-known Kora Volcano generated several structural traps including piercement domes, drag folds, upturned pinchouts and jacked up sedimentary strata above magmatic intrusions. Thus, a better delineation of these subsurface structures using our DSMF volume opens up new opportunities for hydrocarbon exploration within the magmatic region of the northern Taranaki Basin. Furthermore, we ascertain that volume of the folds can be calculated with better precision using the DSMF volume obtained through this research.

The study of magmatic deformation processes also adds value to the exploration of geothermal energy. This study reveals the presence of a hydrothermal vent complex in the NW part of the prospect (Figs. 8c and e). Hydrothermal vents lie below Fold B, where seismic signal appears to be washed out (Figs. 8c and e). These inference patterns suggest that the hydrothermal vent complex below Fold B, reflecting magmatic sills below this fold, ensures the continuity of superheated fluid circulation in the NW part of the Kora Volcanic Complex. Its detailed study may open up wider opportunities for the exploration and exploitation of geothermal resources in the northern Taranaki Basin.

6. Conclusions

An acoustically enhanced depth-converted seismic volume allowed us to investigate the age and geometry of forced folds associated with the intrusion of sills around the Kora volcano, Taranaki Basin, New Zealand. The main conclusions of this work are summarised as:

1. The intrusion of saucer-shaped sills around the Kora Volcanic Complex of the Taranaki Basin resulted in the growth and development of forced folds within the Upper Cretaceous-Paleocene strata. These strata are significantly older than intervals in which forced folds were previously identified literature, within the Kora Volcanic Complex.
2. The interpreted geologic horizon lying immediately above the intruded sills presents two distinct forced folds: Folds A and B. Fold A is developed at the central part of the interpreted seismic volume, whereas Fold B lies at a distance of ~ 5 km from Fold A, towards the NW.
3. The sill-fold relationships in this work demonstrate that the structure and geometry of the forcing member plays a significant role in the development of forced folds. For a successful intrusion of saucer-shaped sills, the ratio of sill length to intrusion depth (L/D) ratio should range from two (2) to six (6).
4. The intrusion of magmatic sills around the Kora Volcanic Complex uplifted the overlying strata generating Folds A and B, which show structural reliefs ranging from 250 m to 350 m.
5. Uplift of overburden strata generated suitable hydrocarbon traps in subsurface units. Moreover, the presence of hydrothermal vent complexes in the NW part of the Kora Volcanic Complex opens new leads in terms of geothermal energy production.

Acknowledgements
This is a collaborative work carried out by Wadia Institute of Himalayan Geology (WIHG), Dehradun and 3D seismic Lab, Cardiff University UK. The New Zealand Petroleum and Minerals and the dGB Earth Sciences are vehemently thanked for providing the valuable data and software support for academic research. Marine Seismic Group, CSIR-NGRI is acknowledged for helping the first author during his doctoral work. The Director, WIHG is acknowledged for permission to publish this work. This is a Wadia contribution No: WIHG/0030. Reviewers XXX and YYY and editor ZZZ are thanked for their constructive comments on an earlier version of this work.

References

Alves, T.M., Omosanya, K.D., Gowling, P., 2015. Volume rendering of enigmatic high-amplitude anomalies in southeast Brazil: A workflow to distinguish lithologic features from fluid accumulations. Interpretation 3: A1-A14.

ARCO Petroleum, 1988. Final well report, Kora-1 and Kora-1A, PPL 38447, Ministry of Economic Development New Zealand. Unpublished Petroleum Report Series, PR 1374, 1–885.

Bischoff, A. P., Andrew, N., Beggs, M., 2017. Stratigraphy of architectural elements in a buried volcanic system and implications for hydrocarbon exploration. Interpretation, 5, SK141-159.

Bussell, M. A., 1989. A simple method for the determination of the dilation direction of intrusive sheets. J. Struc. Geol., 11, 679-687.

Cartwright, J., Huuse, M., 2005. 3D seismic technology: the geological 'Hubble'. Basin Res. 17, 1-20.

Chopra, S., Marfurt, K. J., 2007. Seismic attributes for prospect identification and reservoir characterization. SEG, Tulsa.

Cukur, D., Horozal, S., Kim, D.C., Lee, G.H., Han, H.C. and Kang, M.H., 2010. The distribution and characteristics of the igneous complexes in the northern East China Sea Shelf Basin and their implications for hydrocarbon potential. Marine Geophysical Researches, 31(4), 299-313.

du Toit, A. I., 1920. The Karoo dolerites. Trans. Geol. Soc. S. Africa., 33, 1-42.

Eide, C.H., Schofield, N., Lecomte, I., Buckley, S.J., Howell, J.A., 2017. Seismic interpretation of sill complexes in sedimentary basins: implications for the sub-sill imaging problem. J. Geol. Soc. 2017-096.

Fialko, Y., 2001. On origin of near-axis volcanism and faulting at fast spreading mid-oceanic ridges. Earth. Planet. Sc. Lett., 190, 31-39.

Friðleifsson G. O., Elders, W.A., Albertsson, A., 2014. The concept of the Iceland deep drilling project. Geotherm., 49, 2–8.

Giba, M., Nicol, A., Walsh, J. J., 2010. Evolution of faulting and volcanism in a back-arc basin and its implication for subduction processes. Tectonics, 29, 4, TC4020, 1-18.

Hansen, D.M., Cartwright, J.A., Thomas, D., 2004. 3D seismic analysis of the geometry of igneous sills and sill junction relationships. In: Davies, R.J., Cartwright, J.A., Stewart, S.A., Lappin, M., Underhill, J.R. (Eds.), 3D Seismic Technology: Application to the Exploration of Sedimentary Basins. Geol. Soc., London, 199-208. Memoirs 29.

Hansen, D. M., Cartwright, J. 2006a. The morphology of intrusion-related vent structures and their implications for constraining the timing of intrusive events along the NE Atlantic margin. Journal of the Geological Society, 163**,** 789-800.

Hansen, D. M., Cartwright, J., 2006b. The three-dimensional geometry and growth of forced folds above saucer-shaped igneous sills. J. Struc. Geol., 28, 1520-1535.

Hansen, D. M., Redfern, J., Federici, F., di Biase, D., Bertozzi, G., 2008. Miocene igneous activity in the Northern Subbasin, offshore Senegal, NW Africa. Mar. Pet. Geol., 25, 1-15.

Higgs, K.E., King, P. R., Raine, J. I., Sykes, R., Browne, G. H., Crouch, E. M., Baur, J. R., 2012. Sequence stratigraphy and controls on reservoir sandstone distribution in an Eocene marginal marine-coastal plain fairway, Taranaki Basin, New Zealand. Mar. Pet. Geol., 32, 110-137.

Hotz, P.E., 1952. Form of diabase sheets in south eastern Pennsylvania. American Journal of Science 250, 375-388.

Hutton, D. H. W., 2009. Insights into magmatism in volcanic margins: bridge structures and a new mechanism of basic sill emplacement-Theoren Mountains, Antarctica. Petrol. Geosci., 15, 269-278.

Infante-Paez, L., Marfurt, K. J., 2017. Seismic expression and geomorphology of igneous bodies. A Taranaki Basin, New Zealand case study. Interpretation, 5, 1-72.

Jackson, C. A-L, Scofield, N., Golenkov, B., 2013. Geometry and controls on the development of igneous sill–related forced folds: A 2-D seismic reflection case study from offshore southern Australia. Geol. Soc. of America Bull. doi:10.1130/B30833.1

Jackson, C. A-L, 2012. Seismic reflection imaging and controls on the preservation of ancient sill-fed magmatic vents. J. Geol. Soc., 169, 503-506.

King, P.R., Thrasher, G.P., 1996. Cretaceous-Cenozoic geology and petroleum systems of the Taranaki Basin, New Zealand: Institute of geological and Nuclear Sciences, Lower Hutt (N.Z.) Monograph 13.

King, P. R., Naish, T. R., Browne, G. H., Field, B. D., Edbrooke, S. W. 1999. Cretaceous to Recent sedimentary patterns in New Zealand. Institute of Geological & Nuclear Sciences Folio Series 1 Lower Hutt: Institute of Geological & Nuclear Sciences.

King, P.R., 2000. Tectonic reconstructions of New Zealand: 40 Ma to the present. N. Z. J. Geol. Geophys. 43, 611-638.

Kumar, P.C., Omosanya, K. O., Sain, K., 2019a. Sill Cube: An automated approach for the interpretation of magmatic sill complexes on seismic reflection data. Mar. Pet. Geol., 100, 60-84.

Kumar, P.C., Sain, K. and Mandal, A. 2019b. Delineation of a buried volcanic system in Kora prospect off New Zealand using artificial neural networks and its implications. J. App. Geophys., 161, 56-75.

Kumar, P.C., Omosanya, K.O., Alves, T. and Sain, K. 2019c. A neural network approach for elucidating fluid leakage along hard-linked normal faults. Mar. Pet. Geol., 110, 518-538.

Liotta, D., Brogi, A., Meccheri, M., Dini, A., Bianco, C., Ruggieri, G., 2015. Coexistence of low-angle normal and high-angle strike-to oblique-slip faults during Late Miocene mineralization in eastern Elba Island (Italy). Tectonophy., 660, 17–34.

Liu, C., Liu, Y., Yang, B., Wang, D., Sun, J., 2006. A 2D multistage median filter to reduce random seismic noise. Geophysics 71, V105–V110

Loewinson-Lessing, F., 1936. A contributions to the mechanics of intrusions. 16th International Geological Congress Report, 333-352.

Magee, C., Briggs, F., Jackson, C.A-L., 2013a. Lithological controls on igneous intrusion-induced ground deformation: J. Geol. Soc. London, 170, 853–856.

Magee, C., Jackson, C.A-L., Schofield, N., 2014. Diachronous sub-volcanic intrusion along deep-water margins: Insights from the Irish Rockall Basin. Basin Res., 26, 85-105.

Malthe-Sørensen, A., Planke, S., Svensen, H., Jamtveit, B., 2004. Formation of saucer-shaped sills. Geol. Soc., Special Publication 234, London, 215-227.

Montanari, D., Bonini, M., Corti, G., Agostini, A., Del Ventisette, C., 2017. Forced folding above shallow magma intrusions: Insights on supercritical fluid flow from analogue modelling. J. Volcanol. Geotherm. Res., doi: 10.1016/j.jvolgeores.2017.07.022

Morley, C. K., 2018. 3-D seismic imaging of the plumbing system of the Kora Volcano, Taranaki Basin, New Zealand: The influence of syn-rift structure on shallow igneous intrusion architecture. Geosphere, 14, 2533-2584.
Nicholson, R., Pollard, D. D., 1985. Dilation and linkage of en-echelon cracks. J. Struc. Geol., 7, 147-165.
Omosanya, K.O., Johansen, S.E., Eruteya, O.E., Waldmann, N., 2017. Forced folding and complex overburden deformation associated with magmatic intrusion in the Vøring Basin, offshore Norway. Tectonophy. 706, 14-34.
OMV New Zealand Limited, 2005. Kora 3D Seismic, Offshore NZ. Ministry of Economic Development New Zealand, Unpublished Petroleum Report, PR3302.
Palmer, J. A., Andrews, P. R., 1993. Cretaceous-Tertiary sedimentation and implied tectonic controls on structural evolution of Taranaki Basin, New Zealand. In: South Pacific Sedimentary Basins: Sedimentary Basins of the world, 2, 309-328, Elsevier, Amsterdam.
Pollard, D. D., Johnson, A. M., 1973. Mechanics of growth of some laccolithic intrusions in the Henry Mountain, 18. Bending and failure of overburden layers and sill formation. Tectonophy., 311-354.
Polteau, S., Mazzini, A., Galland, O., Planke, S., Malthe-Sørenssen A., 2008. Saucer-shaped intrusions: Occurrences, emplacement and implications. Earth and Planetary Science Letters, 266, 195–204.
Sani F., Bonini M., Montanari D., Moratti G., Corti G., Del Ventisette C., 2016. The structural evolution of the Radicondoli–Volterra Basin (southernTuscany, Italy): Relationships with magmatism and geothermal implications. Geotherm., 59, 38–55.
Schofield, N.J., Brown, D.J., Magee, C., Stevenson, C.T., 2012. Sill morphology and comparison of brittle and non-brittle emplacement mechanisms. J. Geol. Soc.169, 127-141.
Schofield, N., Holford, S., Millett, J., Brown, D., Jolley, D., Passey, S.R., Muirhead, D., Grove, C., Magee, C., Murray, J., Hole, M., 2017. Regional magma plumbing and emplacement mechanisms of the Faroe-Shetland Sill Complex: implications for magma transport and petroleum systems within sedimentary basins. Basin Res. 29, 41-63.
Schutter, S. R., 2003. Hydrocarbon occurrence and exploration in and around igneous rocks. Geol. Soc. Lond. Spe. Publ. 7-33.
Scott S., Driesner T., and Weis P., 2015. Geologic controls on supercritical geothermal resources above magmatic intrusions. Nature Comm. 6: 7837. doi:10.1038/ncomms8837
Seebeck, H. C., Nicol, A., Villamor, P., Ristau, J., Pettinga, J., 2014. Structure and kinematics of the Taupo Rift, New Zealand. Tectonics, 33, 1178-1199.
Smallwood, J.R., Maresh, J., 2002. The properties, morphology and distribution of igneous sills: modelling, borehole data and 3D seismic from the Faroe-Shetland area. Geol. Soc. Lond. Spec. Pub. 197, 271-306.
Stagpoole, V., Funnel, R., 2001. Arc magmatism and hydrocarbon generation in the northern Taranaki Basin, New Zealand, Petroleum Geoscience, 7, 255-267.
Trude, K.J., Cartwright, J.A., Davies, R.J., Smallwood, J.R., 2003. A new technique for dating igneous sills. Geol., 31, 813-816.
Tweto, O., 1951. Form and structure of sills near Pando, Colorado. Geol. Soc. of Am. Bull., 62, 507-532.
Weis, P., 2015. The dynamic interplay between saline fluid flow and rock permeability in magmatic-hydrothermal systems. - Geofluids, 15, 350-371.

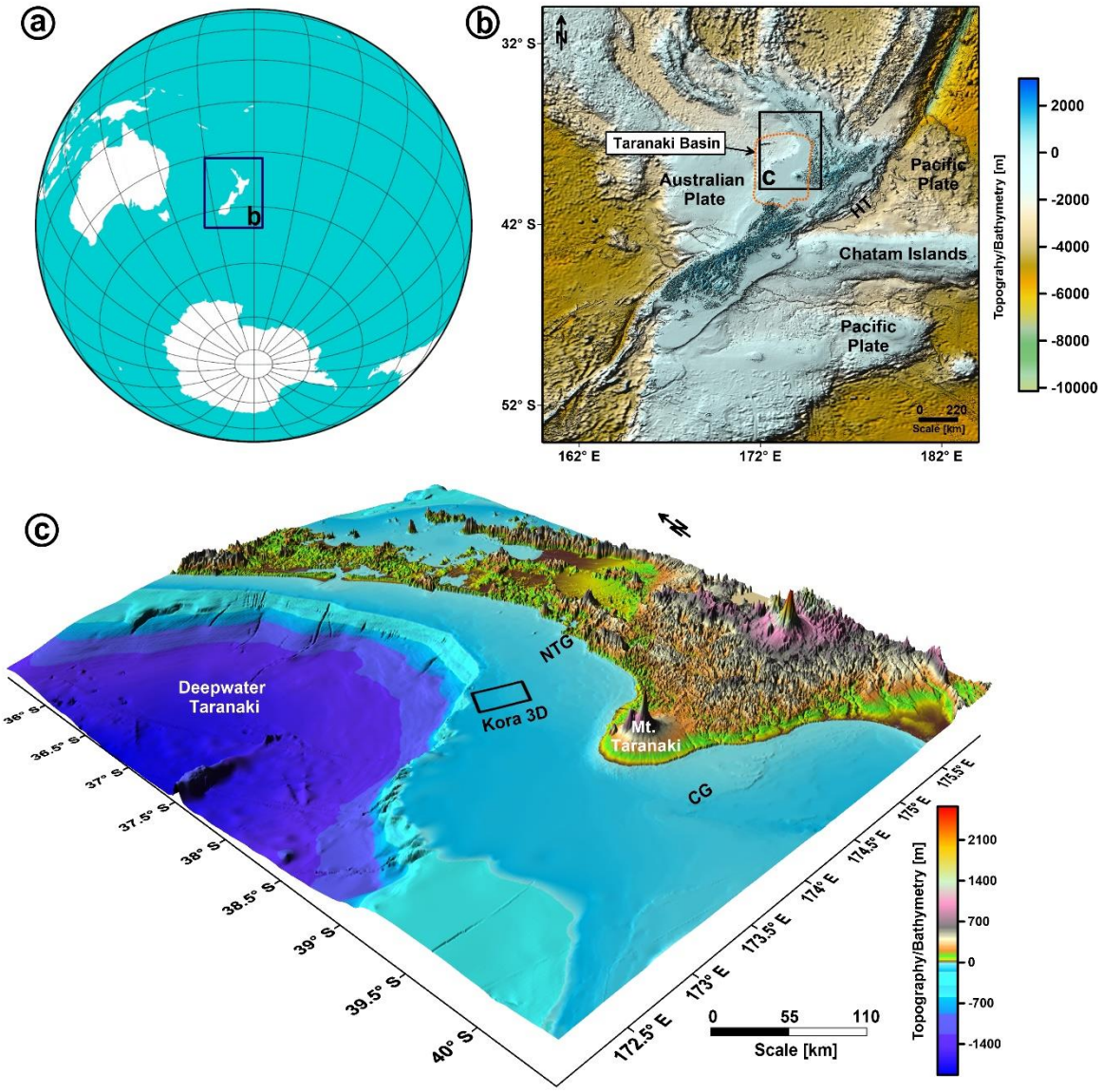

Figure 1: (a) (b) and (c) Taranaki Basin, located offshore New Zealand to the east of the North Island. The basin is demarcated by an orange dotted polygon in Fig. 1b. The Taranaki Basin forms part of the overriding Australian plate and lies west of the Hikurangi Trough, where the Pacific plate is subducted. The Kora 3D seismic volume, highlighted by the black rectangular box in Fig. 1c, lies in the northern part of the basin. NTG: Northern Taranaki Graben, CG: Central Graben.

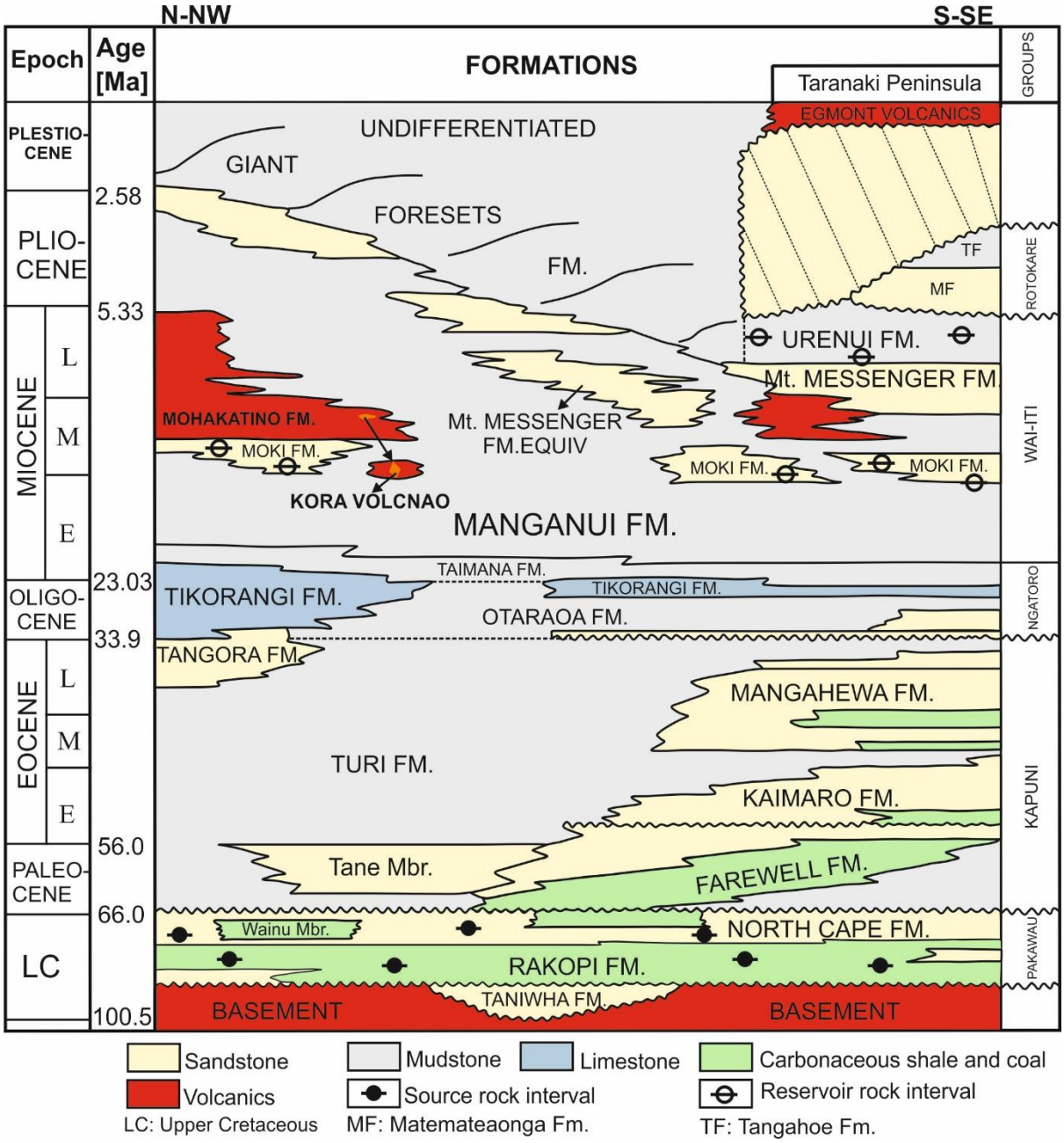

Figure 2: Lithostratigraphic framework of the Taranaki Basin, offshore New Zealand based on King and Thrasher (1996).

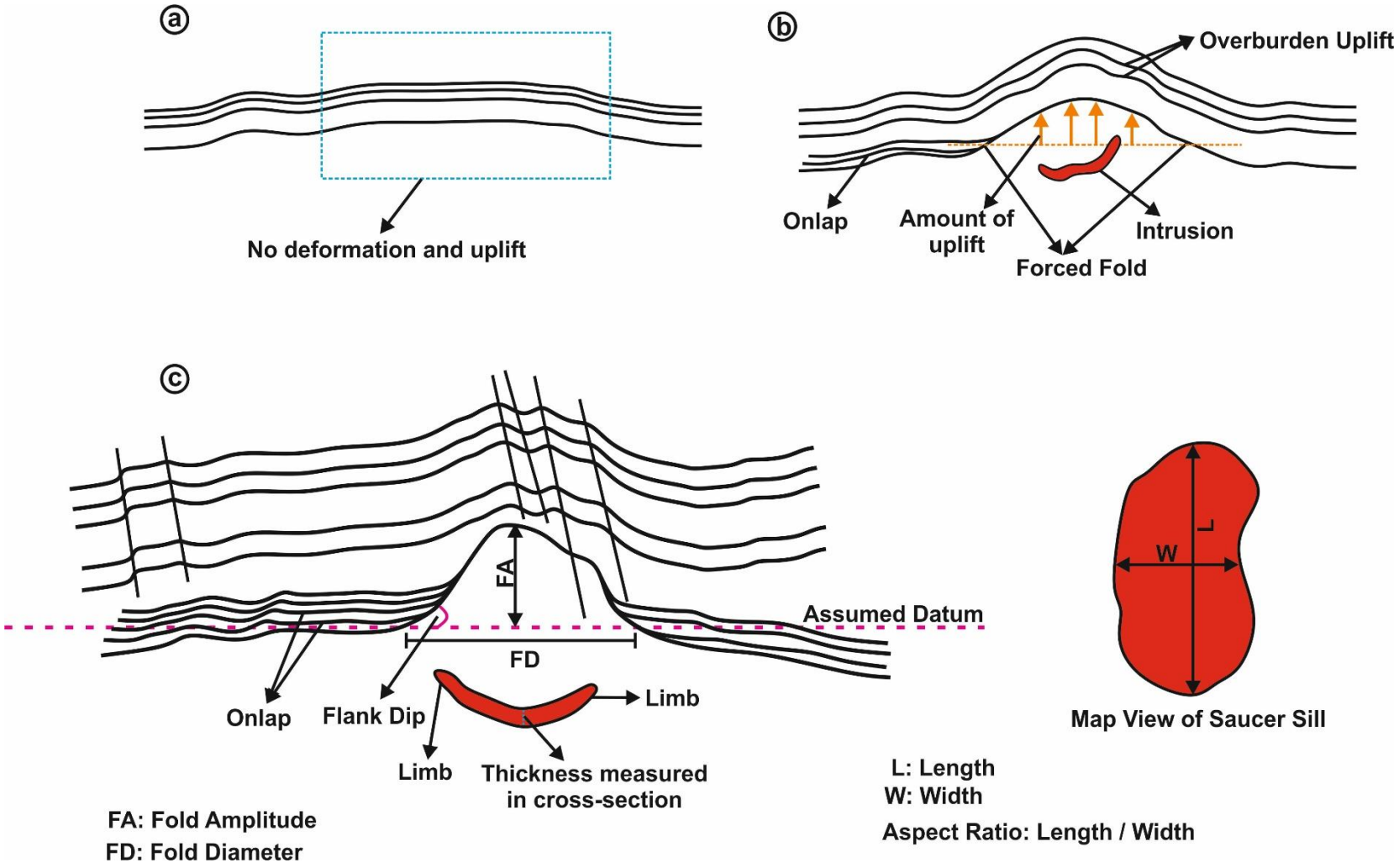

Figure 3: (a) (b) and (c) Schematic representation of subsurface strata summarising the development of forced folds due to the presence of a magmatic sill at depth. The figure also highlights the different morphometric parameters associated with such a deformation.

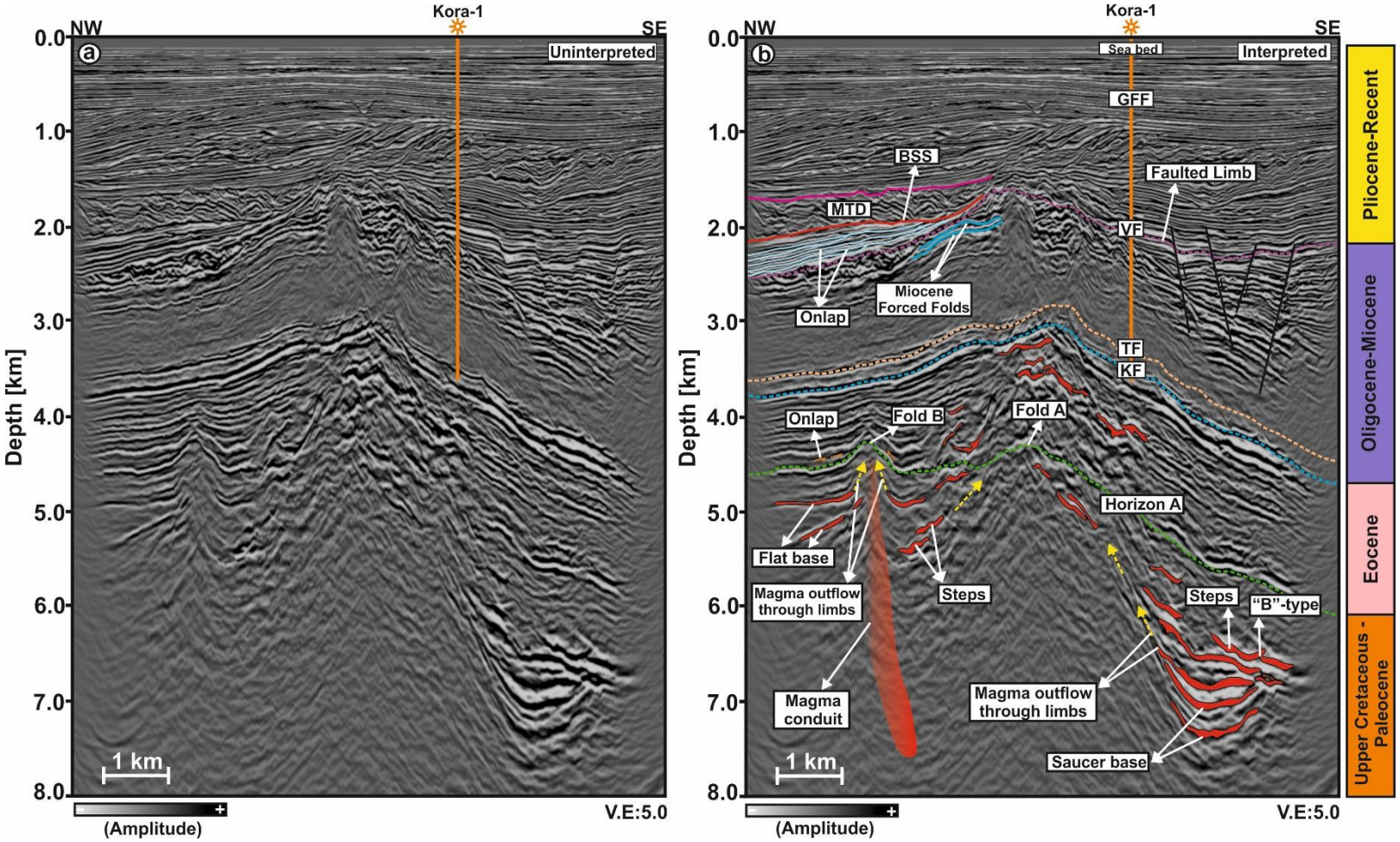

Figure 4: (a) Uninterpreted seismic line IL 1420 and (b) corresponding interpretation showing the subsurface structural framework of the Kora prospect. The Kora-1 well drilled within the prospect terminates at the top of the Eocene strata. The zone of interest for this research comprise Upper Cretaceous-Paleocene deposits that are intruded by a network of magmatic sill. Two distinctive folds named Fold A and Fold B are observed above the intruded sills within the interval of interest. The term VF concerns the well-known Kora Volcano, which remained active during the Miocene and was draped and onlapped by a thick sedimentary cover; the Great Foresets Formation. FF: Forced Fold; MTD: Mass-Transport Deposit; BSS: Basal Shear Surface; GFF: Giant Foreset Formation; VF: Volcanic Formation; TF: Tangaroa Formation; KF: Kaiata Formation.

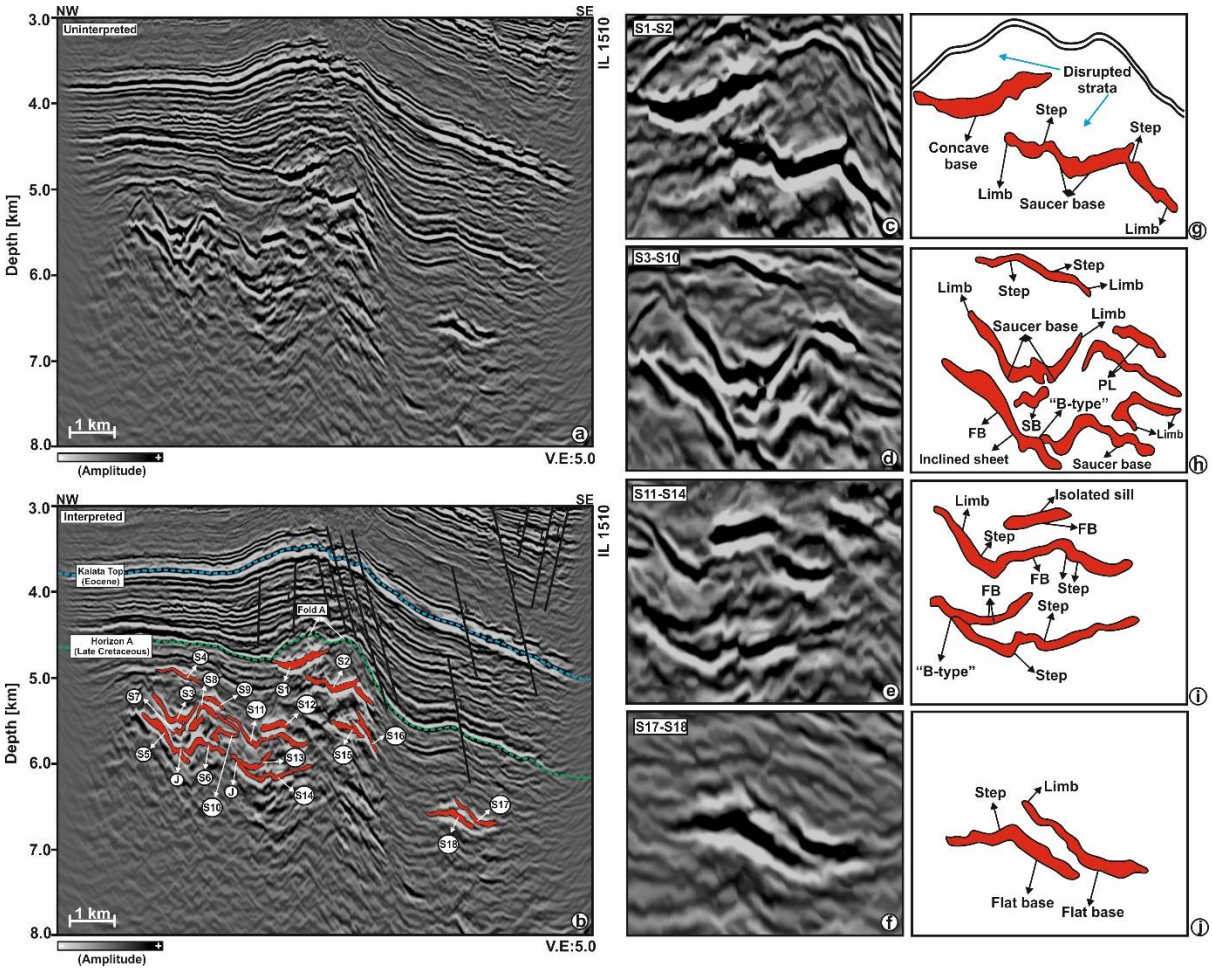

Figure 5: (a) Uninterpreted seismic line IL 1510 and (b) corresponding interpretation highlighting the networks of intruded sills in the subsurface. The zone of interest, Late Cretaceous Horizon A, is marked by a green dotted line. The seismic line highlights the presence of Fold A within stratigraphic Horizon A. The horizon is overlain by thick strata among which is the Eocene Kaiata Formation; see top marked by blue dotted line. The subsurface units are structured by sets of extensional faults. The identified sill networks are marked as S1-S18. Sills S1-S18 (c-f) are interpreted in the adjacent sketches (g-j) to understand its detailed structural geometry. The interpreted sills demonstrate different structures e.g., saucer-shape, inclined sheets, equally spaced steps, occurring in isolation and with flat bases. SB: Saucer Base; FB: Flat Base; PL: Parallel-layered

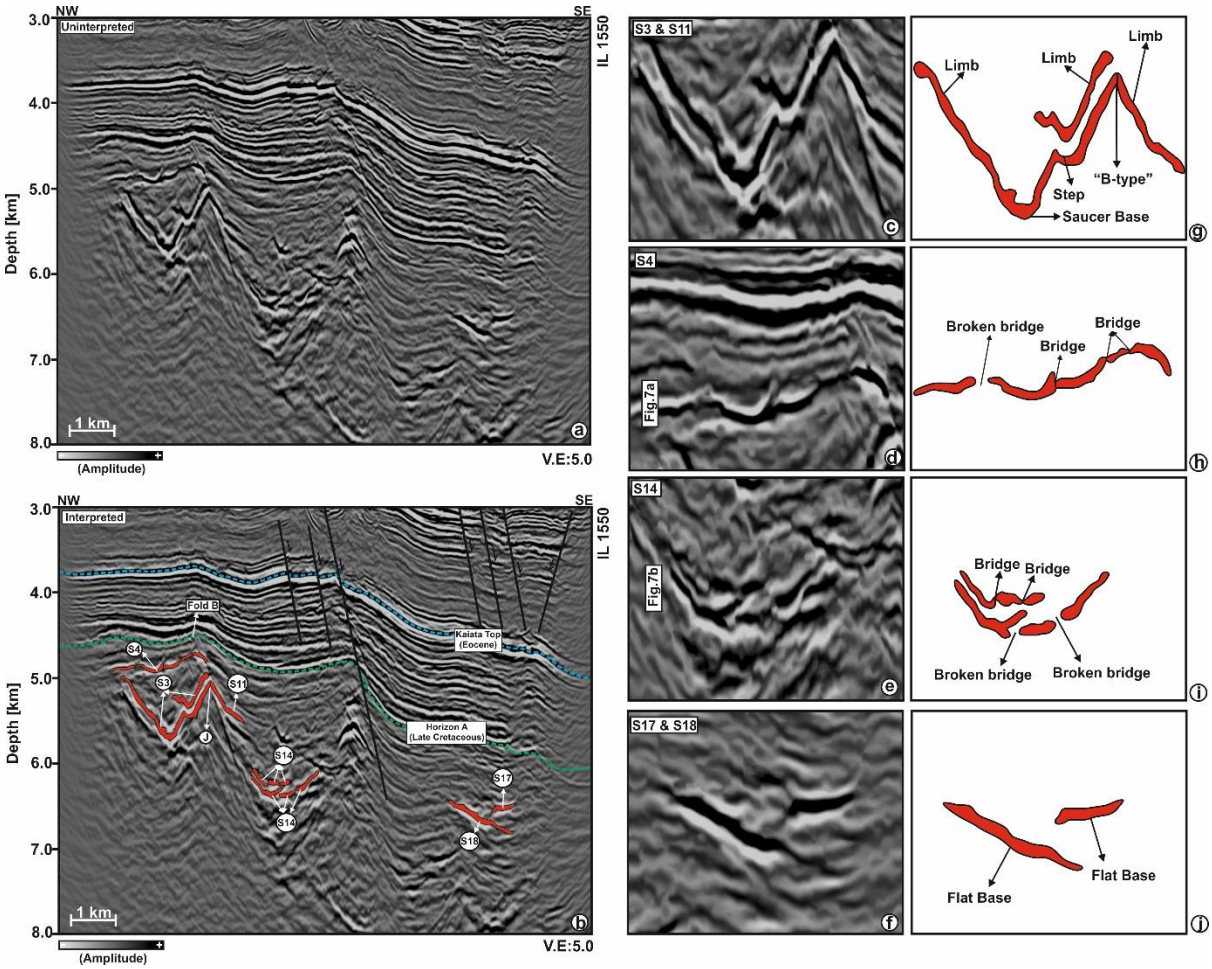

Figure 6: (a) Uninterpreted seismic line IL 1550 and (b) corresponding interpretation revealing networks of intruded sills in the subsurface. The Late Cretaceous Horizon A, is marked using a green dotted line. The seismic line distinctly highlights the presence of Fold B structure within the stratigraphic Horizon A. Sills S3, S4 & S11 lie below Fold B. Sill S14 lies at a deeper level in the central part of the seismic line. Sills S17 & 18 lie at deeper levels towards the SE. The identified sills (c-f) are interpreted in the adjacent sketches (g-j) to ascertain its detailed structural geometry. The interpreted sills demonstrate different geometries e.g., saucer-shape, inclined sheets, broken-bridge structures and sill-sill junctions.

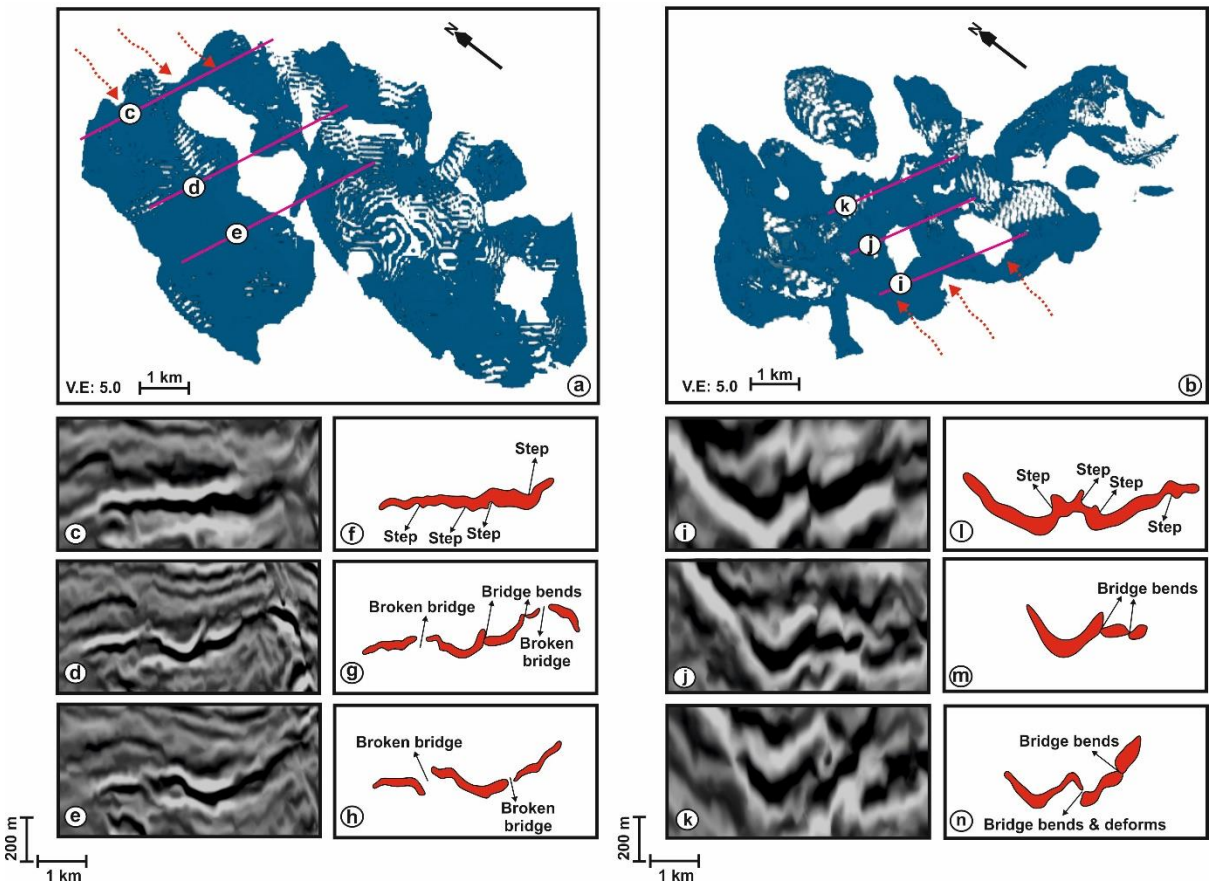

Figure 7: (a) Opacity rendered volumetric display of sill S4. Sill S4 consists of en echelon magma lobes (arranged in steps) and are associated with broken bridge structures. Different seismic profiles (c-e) and corresponding interpretations (f-h) illustrates the development of broken bridge structures in sill S4. Pink dotted arrows in (a) indicate the direction of magma flow; (b) Opacity rendered volumetric display of sill S14. Sill S14 consists of en echelon magma lobes (arranged in steps) and are associated with broken bridge structures. Seismic profiles (i-k) and corresponding interpretations (l-n) demonstrate the development of broken bridge structures within sill S14. Pink dotted arrows in (b) indicate the direction of magma flow.

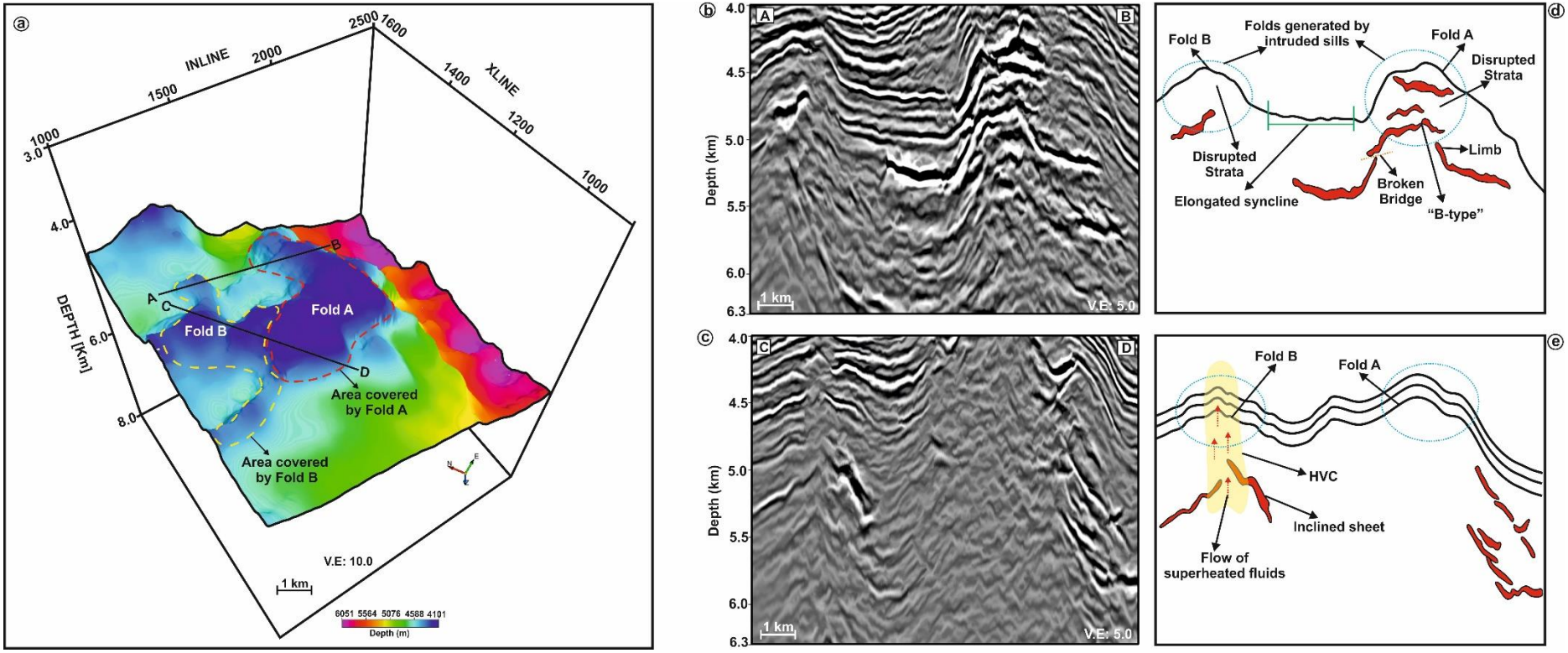

Figure 8: (a) TWT structure map of Horizon A. This seismic horizon shows two major forced folds named Fold A (marked by the red dotted polygon) and Fold B (marked by the yellow dotted polygon). Folds A and B cover an area of ~45 km^2 and 35 km^2, respectively. Seismic profiles (b-c) and their corresponding sketches (d-e) confirm their presence, where the folded structures are intruded by magmatic sills. Fold A occupies the central part of the seismic profile and Fold B lies towards the NW. Both are semicircular. The intrusion of magmatic sills vertically displaces strata, generating the forced folds. A hydrothermal vent complex (HVC) is observed below Fold B suggesting for the flow of superheated fluids through these structures.

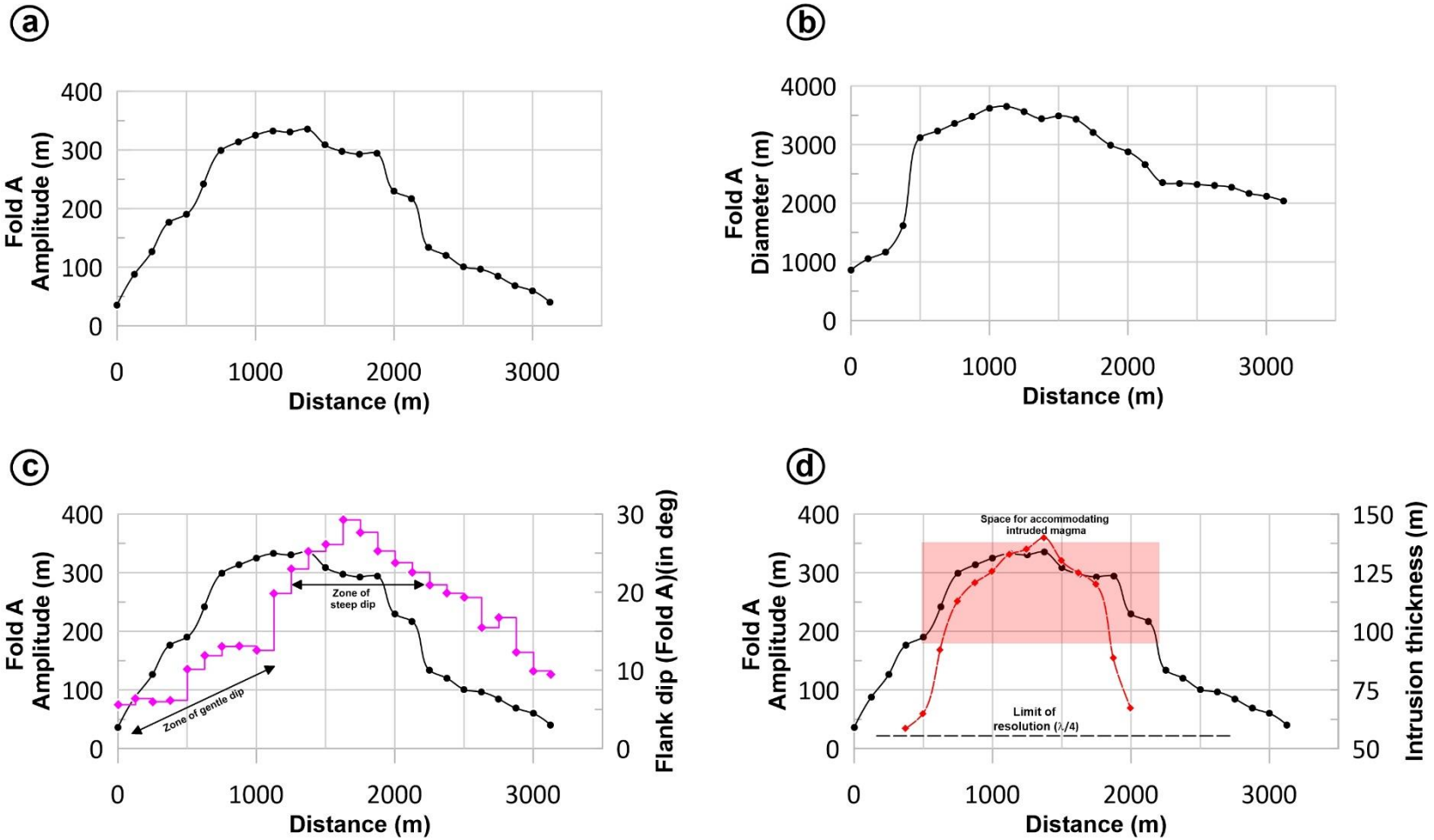

Figure 9: (a-d) Different morphometric parameters (fold amplitude, fold diameter, flank dip, sill thickness) of Fold A and sill S1 measured along cross-sectional transects. The graph shows that the fold exhibits a near-semicircular geometry with a maximum structural relief of ~300 m and an average flank dip of 16^0. The diameter is gently arched. Sill S1 has a maximum intrusion thickness of ~150 m. Fold amplitude and diameter are shown by the black solid line. For flank (or limb of the fold) dip, a step plot is used. The thickness of sill S1 is plotted using a red solid line.

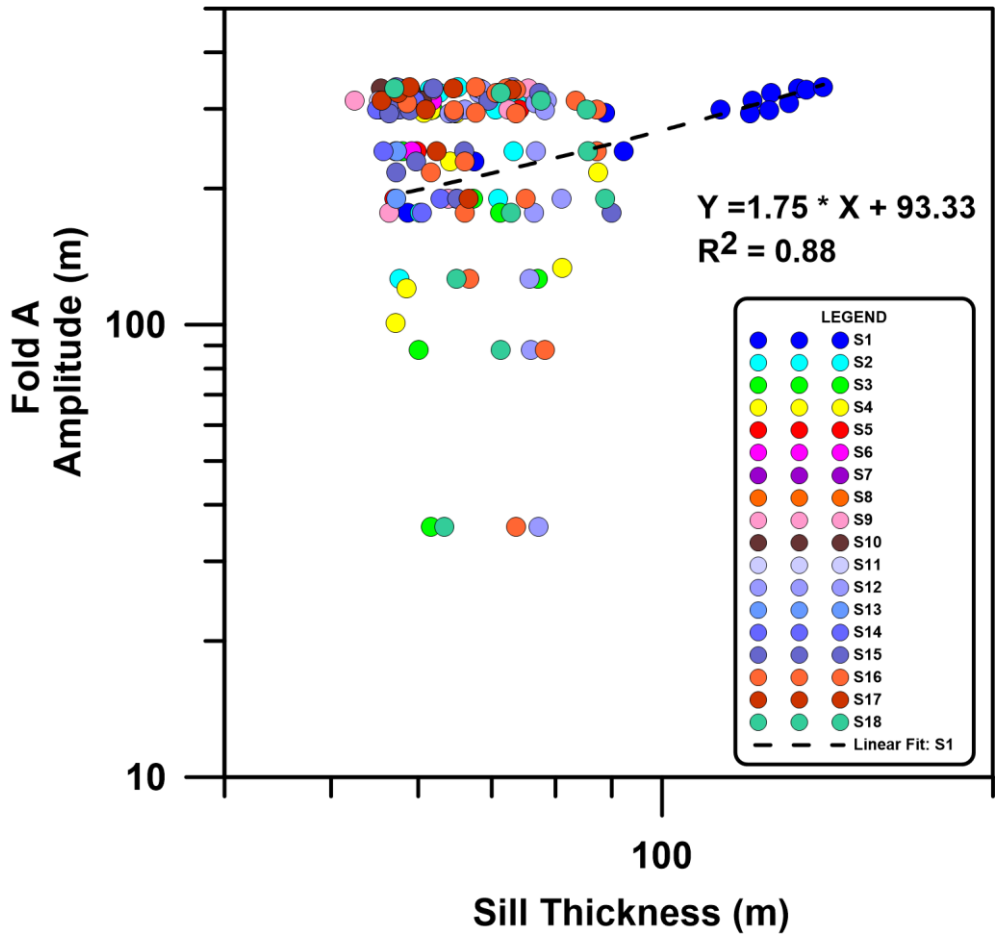

Figure 10: Log-Log plot for Fold Amplitude (Fold A) vs Sill Thickness (n=18). Out of the mapped sills, the plot shows a linear relationship (R^2 =88%) and a good correlation (1:1) between the thickness of sill S1 and the amplitude of the overlying forced fold. However, fold amplitude in is approximately 3-10 times larger than sill thickness when analysing the data shown above.

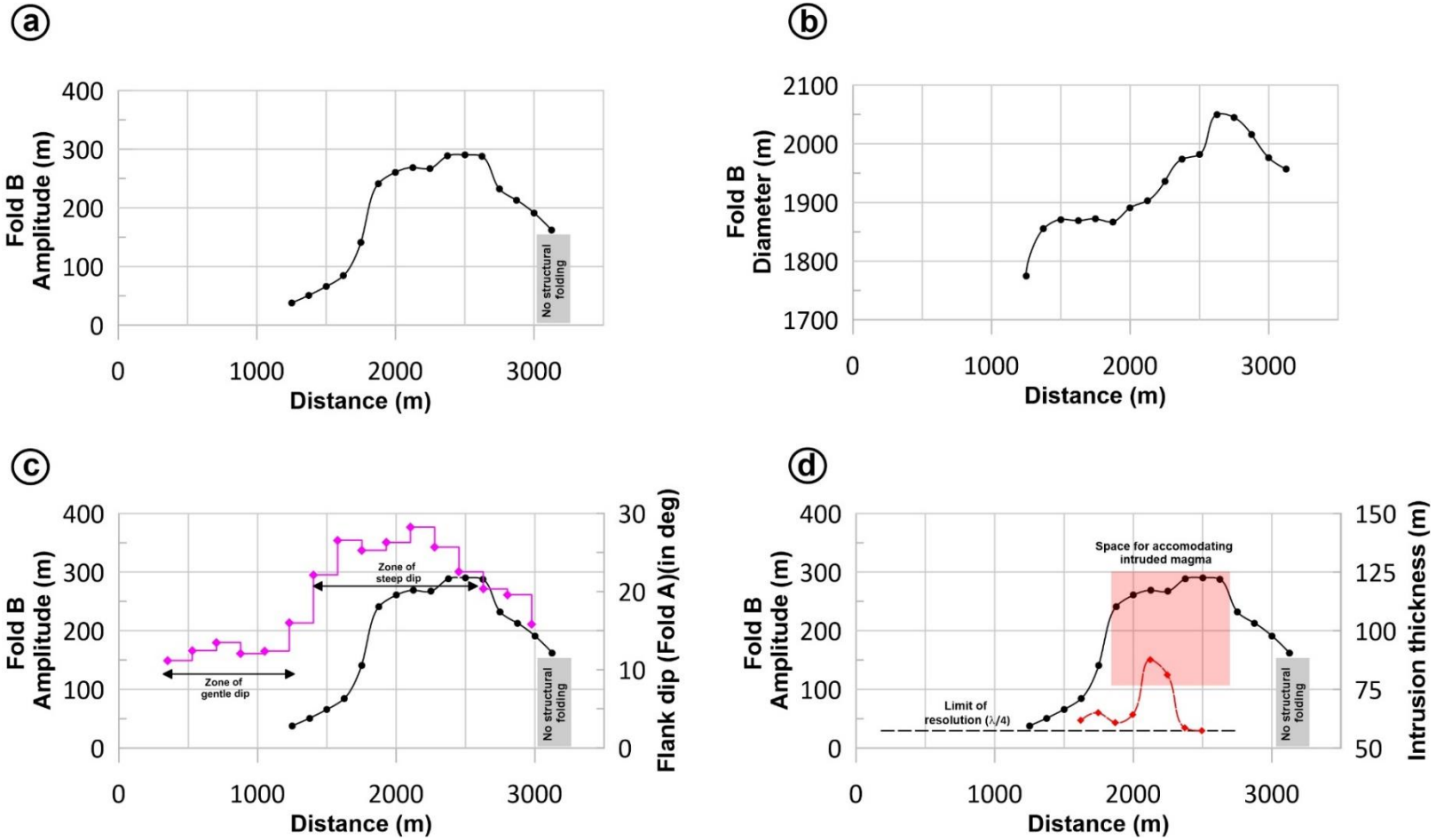

Figure 11: (a-d) Different morphometric parameters (fold amplitude, fold diameter, flank dip, sill thickness) of Fold B and sill S4 measured along cross-sectional transects. The graph shows that the fold exhibits a semicircular geometry and an anticlinal-synclinal-anticlinal (ASA) structure with maximum structural relief of ~290 m and an average flank dip of 19^0. The diameter plot resembles a stepped ladder geometry. Sill S4 has a maximum intrusion thickness of ~87 m. Fold amplitude and diameter are plotted using a black solid line. For the flank (or limb of the fold) dips, a step plot is used. The thickness of sill S4 is plotted using a red solid line.

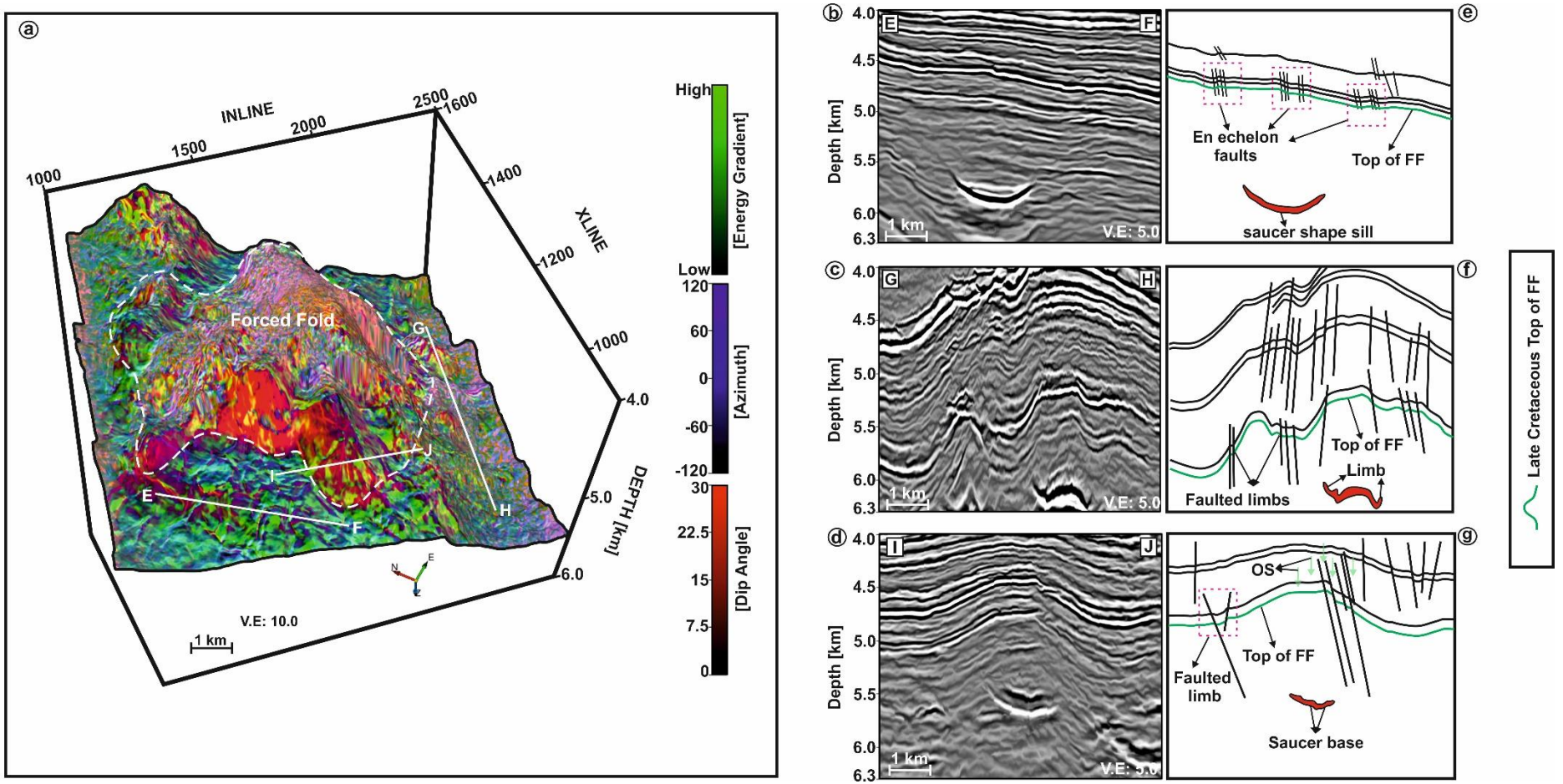

Figure 12: (a) RGB blending of seismic attributes e.g., dip angle, azimuth and energy gradient displayed over Horizon A to visualize fold geometry and its relationship with extensional faults; (b-d) Different seismic transects and corresponding interpreted sketches (e-g) demonstrating the presence of fault networks cross-cutting the Late Cretaceous Horizon A. FF: Forced Fold; OS: Overburden Stress.

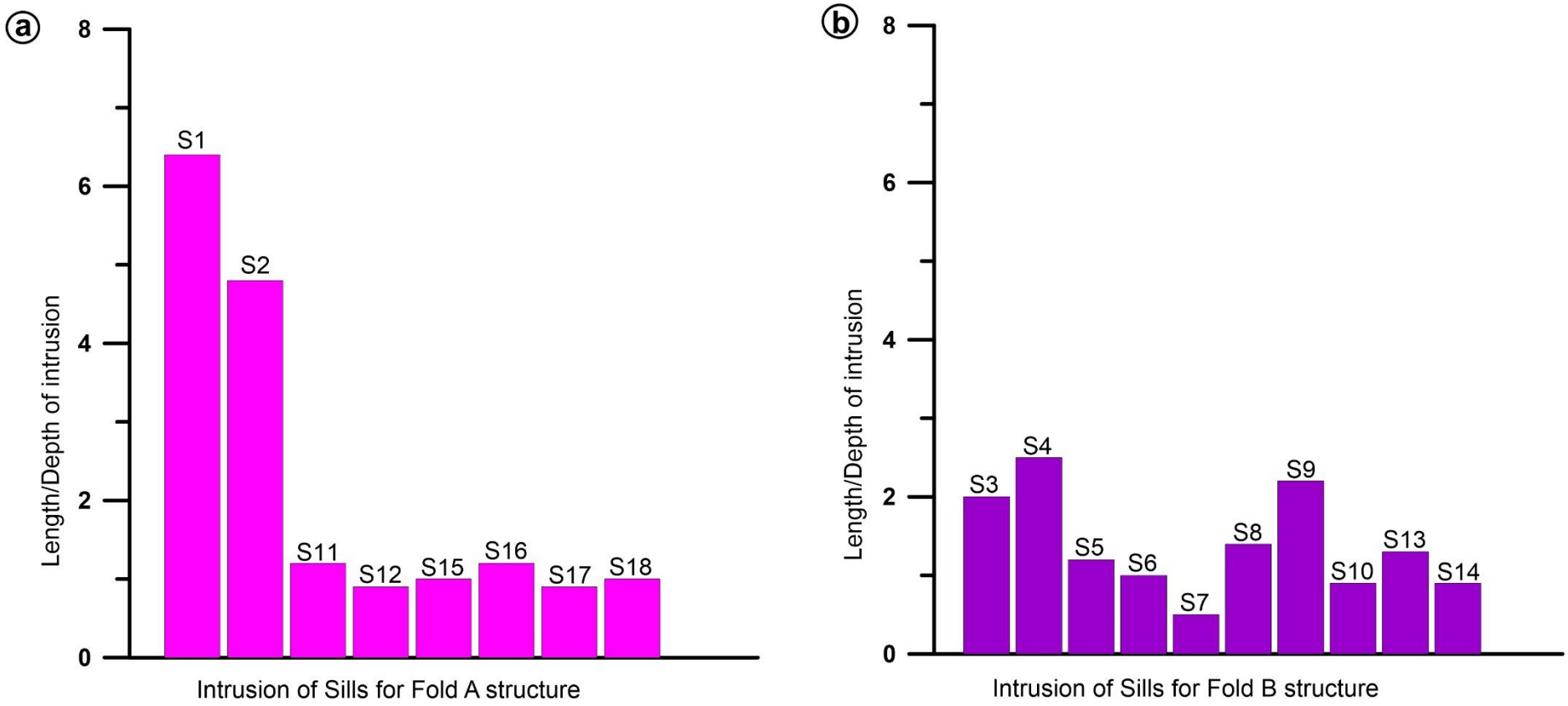

Figure 13: (a) Length to depth of intrusion ratio estimated for sills intruded to generate Fold A. It is observed that sill S1 shows the greatest contribution to forcefully intruding into the host rock to develop Fold A; (b) Length to depth of intrusion ratio estimated for sills that generated Fold B. Sill S4 contributed the most to developing Fold B.

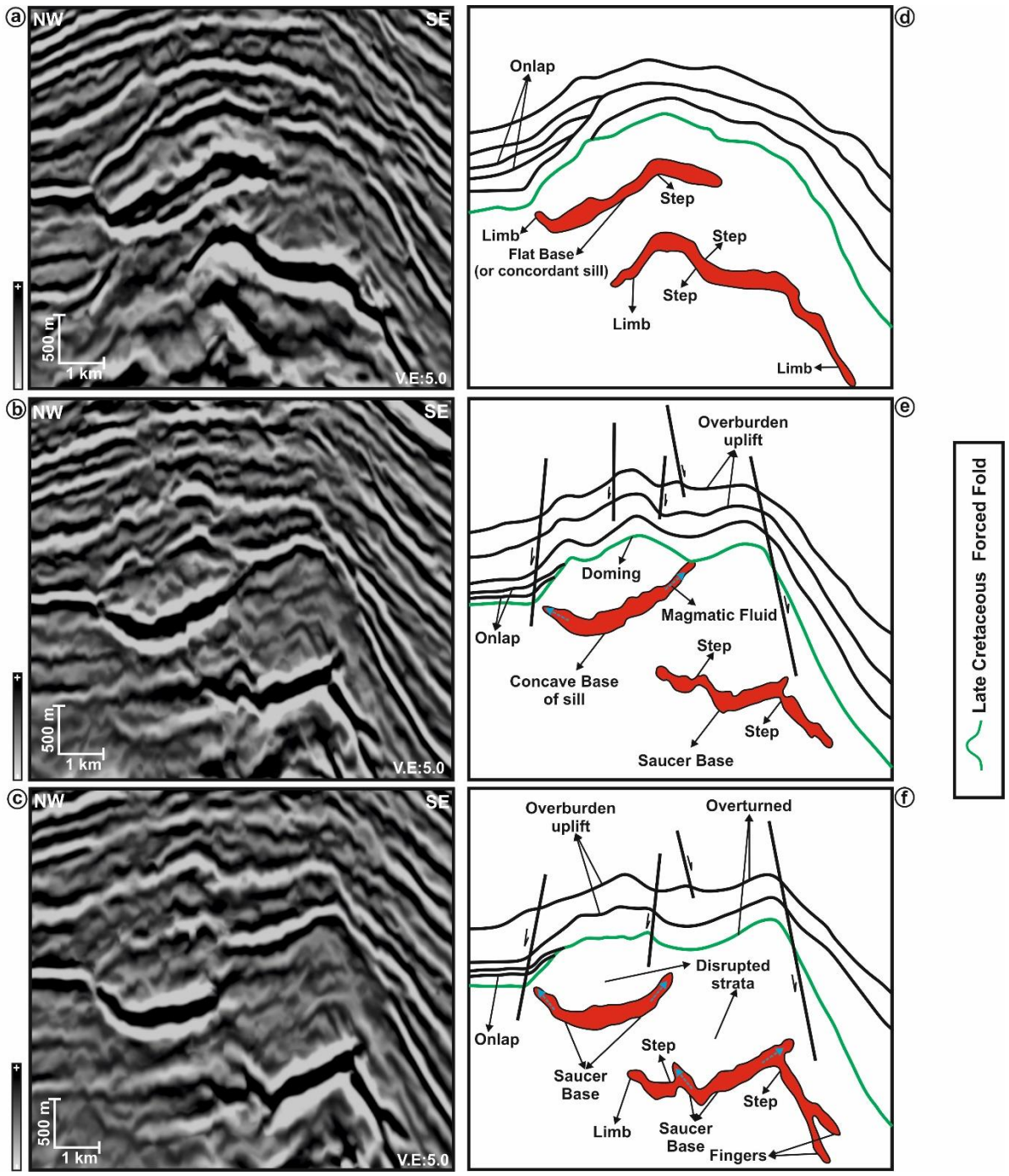

Figure 14: (a), (b) and (c) Growth and development of Fold A due to forceful intrusion of sills S1 and S2; (d), (e) and (f) Corresponding interpreted sketches. Sill S1 intruded at a shallower level in comparison to S2, suggesting that sill S1 contributed the most to the development of Fold A. Gradual development of a saucer shape within sill S1 significantly affected the geometry of adjacent strata, enhancing local deformation to generate Fold A. Fault networks along the flanks accommodate the strain experienced during folding.

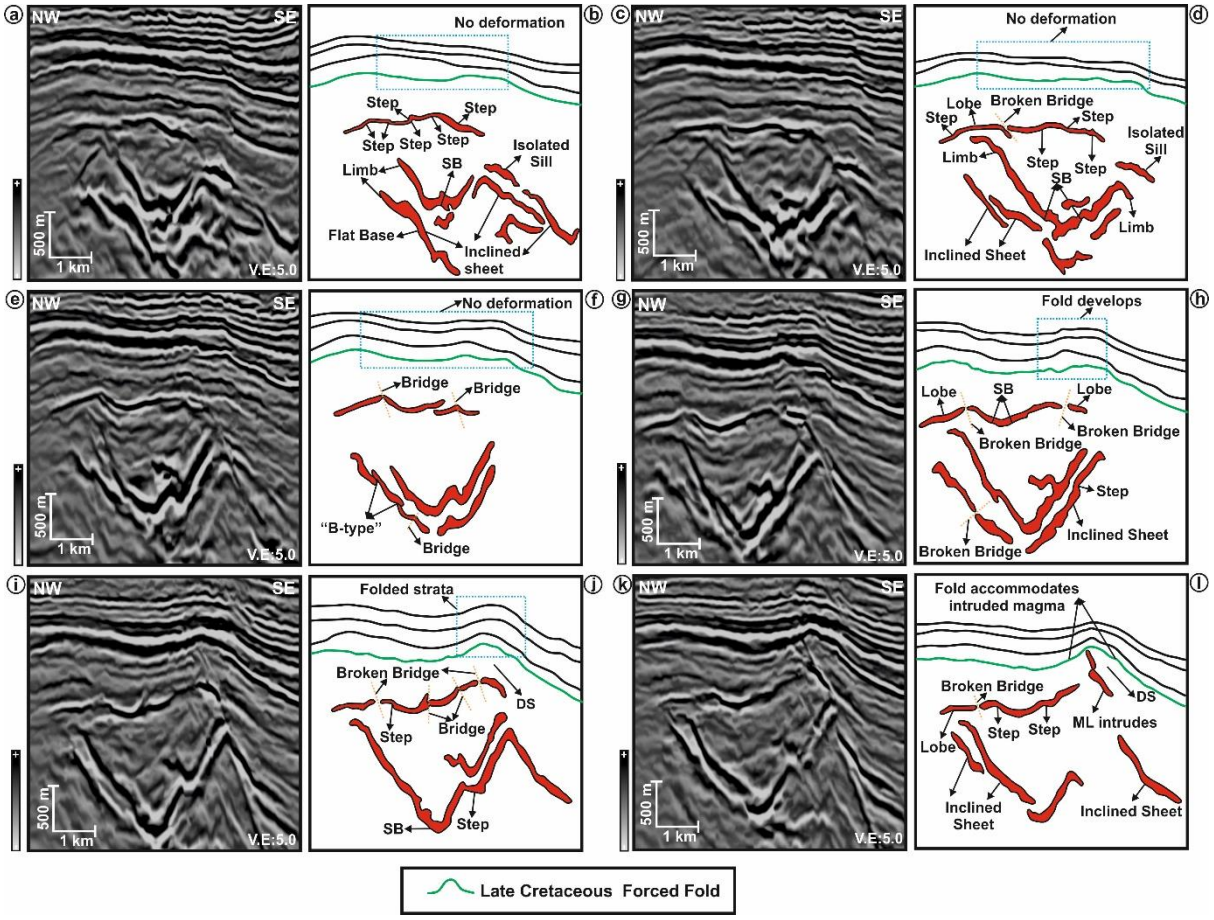

Figure 15: (a-l) Growth and development of Fold B due to the forceful intrusion of sills S4 and S3 revealed by seismic profiles and their interpreted sketches. Sill S4 intrudes at a shallower level in comparison to S3, suggesting it contributed the most to developing Fold B. Sill 4 consists of equally spaced magma lobes associated with broken bridge structures. The movement of magma through these lobes continues to the NW, displacing strata upwards to increase structural relief and generate Fold B. DS: Disrupted Strata; SB: Saucer Base; FA: Fold Amplitude; ML: Magma Lobe.

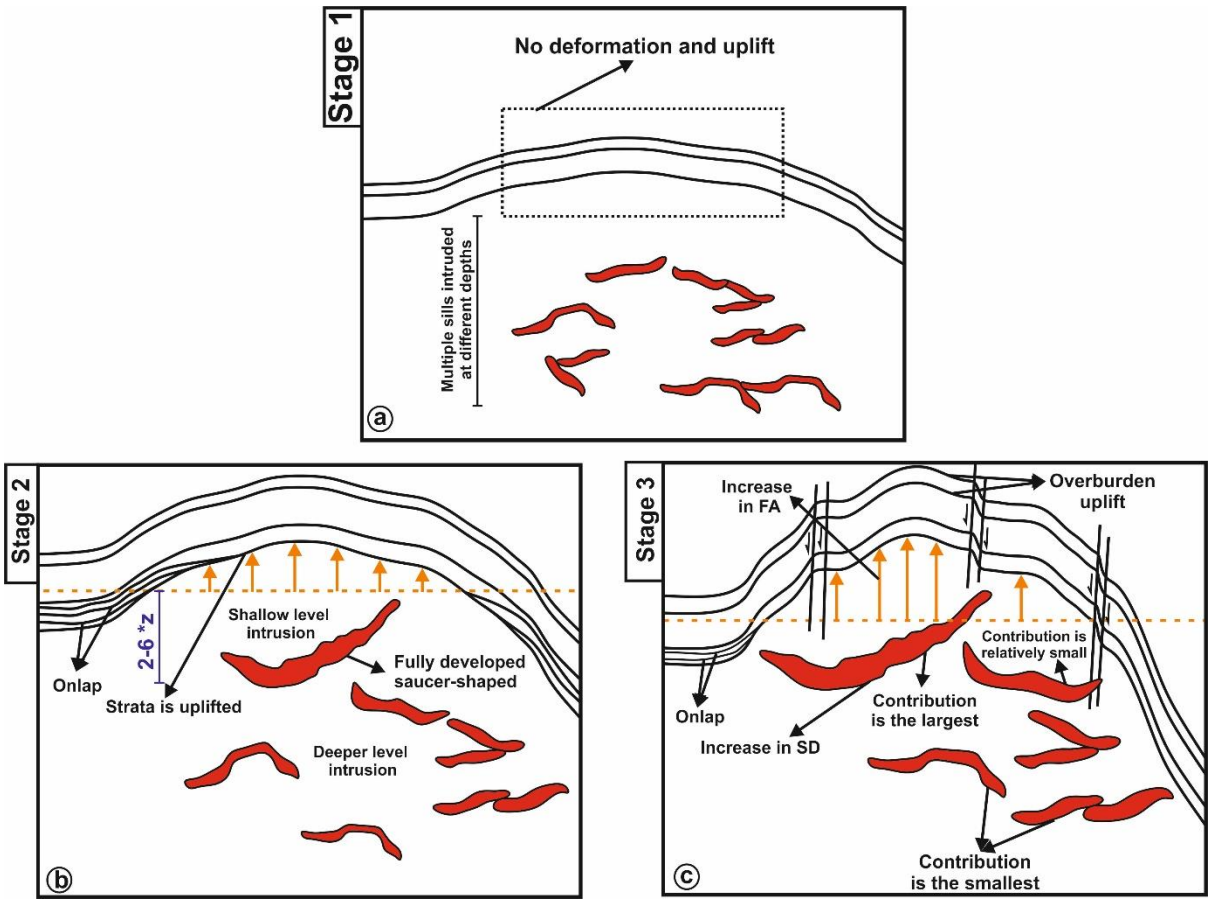

Figure 16: Three-stage conceptual model summarising the relationship between the intruded sills and forced folds in Kora prospect. The figure illustrates the growth and development of the forced fold structures due to the forceful intrusion of saucer-shaped magmatic sills. FA: Fold Amplitude; SD: Sill Diameter.

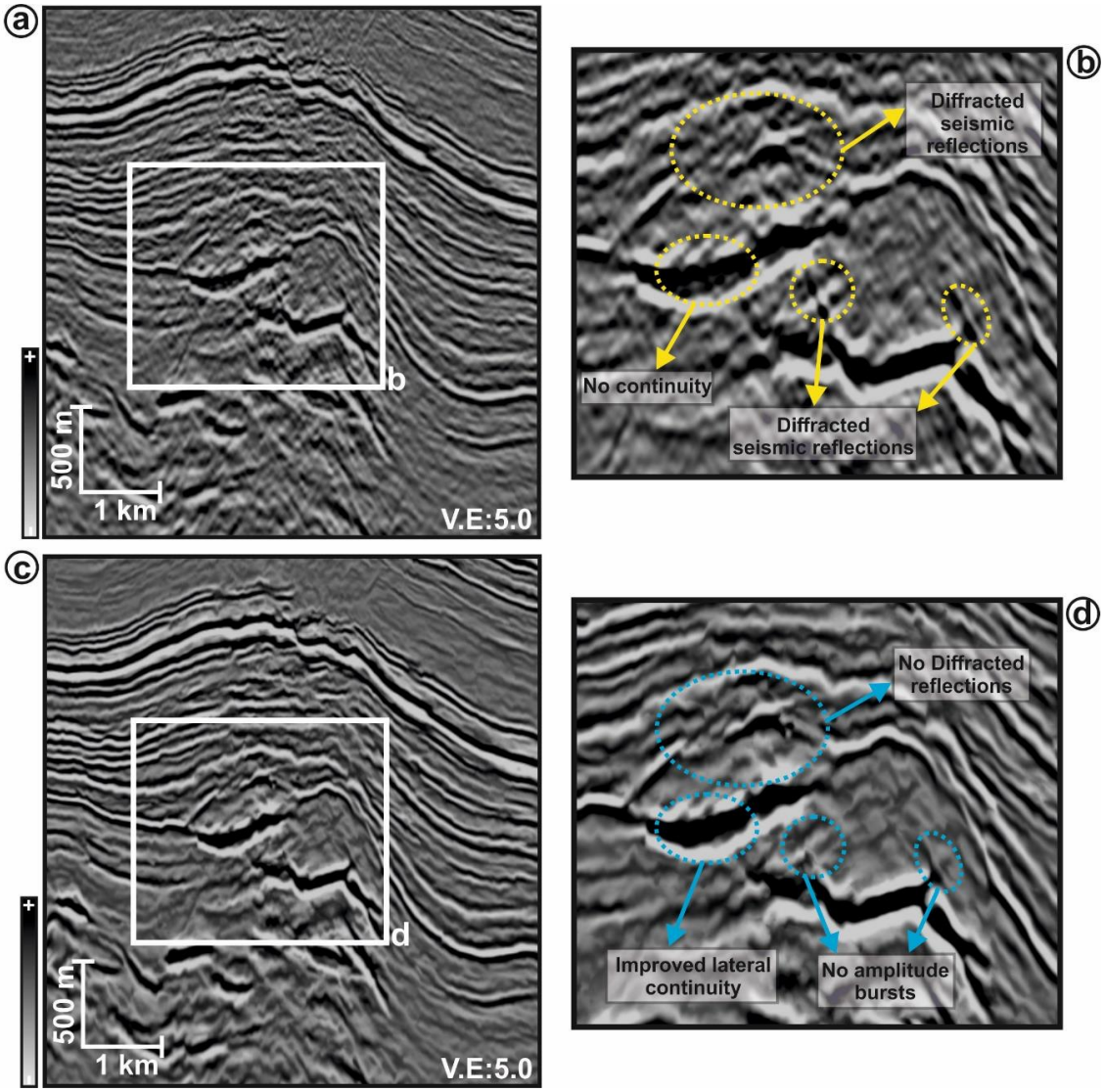

Figure 17: (a) Original seismic line, IL 1500 of the Kora depth migrated seismic cube; (b) zoomed view of this seismic section. The seismic data is prone to noisy reflections leading to poor visualization of magmatic sills and associated structures as is displayed through yellow dotted ovals; (c) DSMF conditioned seismic displayed for the same seismic line IL 1500; (d) Zoomed view of the conditioned seismic section. Structural conditioning improves the subsurface structural imaging of sills and volcanic features. Noise bursts are removed and lateral continuity is enhanced as highlighted by the blue dotted ovals.

Table 1: Sill morphometric parameters. The number of interpreted magmatic bodies reaches a total 18 sills in the study area of the Taranaki Basin, New Zealand.

Sill Name	Structure and Geometry	Orientation	Length (m)	Width(m)	Aspect Ratio
S1	Saucer base with limbs transgressing upwards	NE-SW	1550	636	2.4
S2	Saucer base with limbs associated with steps	NE-SW	2495	1113	2.2
S3	Saucer base with limbs transgressing upwards	NEE-SWW	1823	867	2.1
S4	Flat geometry consisting of en enchelon magma lobes	NNW-SSE	767	841	0.9
S5	Inclined sheet intrusion	N-S	1164	1017	1.1
S6	Inverted saucer structure	NNE-SSW	1172	829	1.4
S7	Flat geometry (saucer pattern is not well developed)	NNW-SSE	581	220	2.6
S8	Inclined sheet-like intrusions	N-S	1031	440	2.3
S9	Inclined sheet-like intrusions	N-S	1374	860	1.6
S10	Inverted saucer structure	NEE-SWW	874	445	2.0
S11	Saucer geometry, flat base with limbs transgressing in steps	NNE-SSW	1176	485	2.4
S12	Occurs in isolation with flat geometry	N-S	667	402	1.6
S13	Flat geometry	NE-SW	1165	987	1.2
S14	Flat base with limbs connected in steps transgressing upwards	NE-SW	1380	682	2.0
S15	Inclined sheet-like intrusion	N-S	1020	426	2.3
S16	Inclined sheet-like intrusion	N-S	984	540	1.8
S17	Occurs in isolation with flat geometry	NE-SW	883	336	2.6
S18	Occurs in isolation with flat geometry	NE-SW	920	410	2.2

Table 2: Thickness of the mapped sills (n=18) in the study area of the Taranaki Basin, New Zealand.

Sill Name	Maximum Thickness (m)	Minimum Thickness (m)	Average Thickness (m)
S1	140.12	58.7	108.28
S2	73.64	57.7	64.99
S3	77.1	57.8	63.357
S4	87.5	57.23	66.972
S5	74.11	57.12	63.676
S6	61.79	58.8	59.93
S7	60.4	57.01	58.705
S8	58.4	57.2	57.8
S9	75.54	55.65	64.287
S10	60.49	55.7	58.366
S11	60.57	55.25	57.91
S12	81.06	64.05	73.656
S13	57.35	55.32	56.696
S14	62.9	55.02	58.75
S15	89.99	56.47	63.712
S16	87.21	58.64	71.918
S17	72.97	55.6	62.4575
S18	88.74	57.04	73.823

Table 3: Forced fold structure, geometry and relative occurrence in the study area.

Fold name	Structure and geometry	Area coverage (km^2)	Occurrence
Fold A	a) Crest with a semicircular geometry b) Limbs widen and are gently arched	45	Occurs in the central part of stratigraphic Horizon A
Fold B	a) Crest with a semicircular geometry and showing a anticlinal-synclinal-anticlinal (ASA) structure b) Limbs gently widen c) Cross-section profile shows a stepped (or ladder) geometry	35	Occurs in the NW part of stratigraphic Horizon A